A CONVERGENT ADAPTIVE FINITE ELEMENT METHOD FOR THE PRIMAL PROBLEM OF ELASTOPLASTICITY

CARSTEN CARSTENSEN*†, ANTONIO ORLANDO†, AND JAN VALDMAN‡

Abstract. The boundary value problem representing one time step of the primal formulation of elastoplasticity with positive hardening leads to a variational inequality of the second kind with some non-differentiable functional. This paper establishes an adaptive finite element algorithm for the solution of this variational inequality that yields the energy reduction and, up to higher order terms, the $R-$linear convergence of the stresses with respect to the number of loops. Applications include several plasticity models: linear isotropic-kinematic hardening, linear kinematic hardening, and multisurface plasticity as model for nonlinear hardening laws. For perfect plasticity the adaptive algorithm yields strong convergence of the stresses. Numerical examples confirm an improved linear convergence rate and study the performance of the algorithm in comparison with the more frequently applied maximum refinement rule.

1. Introduction

The efficient numerical treatment of problems with poor regularity of the solution can be realized with adaptive mesh refinement techniques based on a posteriori error estimators. An $h-$finite element adaptive algorithm consists of succesive loops of the form

$$\text{SOLVE} \to \text{ESTIMATE} \to \text{MARK} \to \text{REFINE} \tag{1.1}$$

designed to produce with less computational effort more efficients meshes by targeted local refinements. The use of the algorithm (1.1), however, is theoretically justified if starting from any initial coarse mesh, one can insure its convergence and establish also the convergence rate. In fact, from approximation theory, it is known that given a separable Hilbert space V and a sequence of finite dimensional subspaces V_ℓ dense in V, the Ritz projection of u onto V_ℓ (and hence the FEM in a typical linear elliptic problem) can converge arbitrarily slow [9]. The convergence analysis of the algorithm (1.1) is, therefore, neither trivial nor implied by the convergence of the FEM but it depends on algorithmic details. In an adaptive finite element method (hereafter referred to as AFEM) the mesh size can stay, in fact, bounded well away from zero. This enforces novel arguments to prove the convergence of AFEMs based on a posteriori error estimates.

* Supported by the DFG Research Center *MATHEON* "Mathematics for key technologies" in Berlin.

Corresponding author: e-mail: cc@math.hu-berlin.de, Phone: +49 2093 5489, Fax: +49 2093 5859.

Date: 5 August 2005.

Key words and phrases. Variational inequality of second kind, elastoplasticity, conforming finite element method, a posteriori error estimates, adaptive finite element methods, error reduction.

The convergence analysis of (1.1) started with the pioneering work of [1] for a two-point elliptic boundary value problem and with the step `MARK` realized by the max refinement rule. This marking rule currently employed in the engineering literature consists in looking at the elements with the largest error and refining these in order to achieve a better accuarcy. Let $\eta^2 := \sum_M \eta_M^2$ denote a typical reliable error estimator with local contributions η_M associated with an edge, face, or element M in the current mesh, the max refinement rule marks a subset $\mathcal{M}$ according to

$$L \in \mathcal{M} \text{ if and only if } \eta_L \geq \Theta \max_M \eta_M \tag{1.2}$$

with $0 \leq \Theta \leq 1$. The analysis of [1], however, does not provide information on the convergence rate and its extension to higher dimensions still remains unsolved. It is only after the contribution of Dörfler [17] with the introduction of a new marking strategy for error reduction (hereafter referred to as bulk criterion or fixed fraction criterion) that the convergence analysis of AFEMs has experienced significant development. With such criterion, one defines the set $\mathcal{M}$ of the marked objects using the rule

$$\sum_{M \in \mathcal{M}} \eta_M^2 \geq \Theta \, \eta^2 \tag{1.3}$$

with $0 \leq \Theta \leq 1$. The condition (1.3) together with local discrete efficiency estimates, and the Galerkin orthogonality yields a linear error reduction rate for the energy norm towards a preassigned tolerance TOL in finite steps for the Poisson problem. In [17] the result was established under the additional condition that the initial mesh was sufficiently refined to resolve data within a certain tolerance, called 'mesh finess'. This condition on the initial mesh, however, is too restrictive since it can produce an initial overrefinement, in contrast with computational experience showing convergence of (1.1) also starting from an initial very coarse mesh. In a series of papers [18, 27, 28, 29] it was realized that the condition on the initial mesh could be removed provided that one can ensure data oscillation reduction. This was achieved by refining with one interior node (rule `bisec5(T)` below) each element marked for error reduction and refine possibly additional elements to enforce a linear oscillation decay. Within the same framework, generalizations to the Raviart-Thomas and to the Crouzeix-Raviart finite element for the Poisson equation have also been considered in [12] and [13], respectively. The lack of conformity and of the Galerkin orthogonality are therein resolved by means of new local discrete efficiency estimates and a quasi-orthogonality condition expressed in terms of data oscillations. In the extension of the analysis to the nonlinear Laplacian, the lack of orthogonality is bypassed in [38] by expressing the problem as a minimization of a suitable energy functional J that allows the discrete error on the energy $J(w_\ell) - J(w_{\ell+1})$ to be related to the discrete error $\|w_\ell - w_{\ell+1}\|^2$ with w_ℓ and $w_{\ell+1}$ conforming finite element approximations on the triangulations $\mathcal{T}_\ell$ and $\mathcal{T}_{\ell+1}$, respectively. The condition (1.3) together with the reliability estimate, the boundeness of J from below, and the observation that $(J(w_\ell))_{\ell \in \mathbb{N}}$ is a Cauchy sequence concludes the convergence of the adaptive algorithm. This analysis, however, does not provide information on the convergence rate. Based also on (1.3) [9] presents a thorough convergence analysis of conforming adaptive finite element methods for uniformly convex and degenerated

(i.e. not strictly) convex differentiable minimization problems, with applications to relaxed microstructures.

In this paper we also adopt (1.3) and we aim at a proof of convergence of AFEM with indication of the rate of convergence for the primal formulation of plasticity. Applications include several plasticity models: linear isotropic-kinematic hardening, linear kinematic hardening, multisurface plasticity as model for nonlinear hardening laws, and perefct plasticity. Following ideas of [38, 9] the problem is transformed in the minimization of a uniformly convex functional J. At variance of those works, however, the energy functional J is not differentiable. Exploiting properties of J, the bulk criterion (1.3), and the reliability of a new edge-based residual error estimate, we obtain the following results:

(*i*) *Energy reduction*: for some data oscillations $\mathrm{osc}_\ell^2 \geq 0$ and positive constants ρ_E, C with $\rho_E < 1$ there holds

$$J(w_{\ell+1}) - J(w) \leq \rho_E(J(w_\ell) - J(w)) + C\mathrm{osc}_\ell^2 \,.$$

(*ii*) *R−linear convergence for the stresses*: up to oscillation terms there holds

$$|||\sigma - \sigma_\ell|||_{\mathbb{C}^{-1};\Omega} \leq \alpha_\ell \quad \text{for } \ell = 0, 1, 2 \cdots ,$$

with $\alpha_\ell \to 0$ and linear convergent, and $|||\cdot|||_{\mathbb{C}^{-1};\Omega}$ the energy norm induced by the Hook tensor $\mathbb{C}$.

Unlike [27, 29] that consider an element-based data oscillation, we consider the node-patchwise definition of the data oscillation proposed by [8]. Such definition arises naturally from the reliability estimate and discloses the role of the data oscillation on the error reduction. Using a criterion similar to (1.3) for the control of the oscillations, we also establish the following result:

(*iii*) *Oscillation reduction*: there exists a positive constant $\rho < 1$ such that

$$\mathrm{osc}_{\ell+1}^2 \leq \rho\, \mathrm{osc}_\ell^2 \,.$$

The remaining part of the paper is organised as follows. Section 2 introduces the primal problem of elastoplasticity. Each time step of the initial boundary value problem results in a boundary value problem expressed as a variational inequality and equivalently as a minimization of a uniformly convex nondifferentiable functional for plasticity models with positive hardening. Section 3 presents a general class of plasticity models that can be treated within the present framework. Section 4 describes the steps `SOLVE` and `ESTIMATE` with the introduction of the edge based residual error estimate and proof of its reliability. The steps `MARK` and `REFINE` are introduced in Section 5 together with the complete adaptive algorithm. The main results of the paper on the energy reduction, the oscillation reduction, and the R-linear convergence of the stresses are given in Section 6 together with the proof of strong convergence of the stresses in the case of perfect plasticity. Numerical examples with applications to the two-yield multisurface plasticity and to a benchmark problem with perfect plasticity validate our theoretical findings in Section 7 whereas Section 8 concludes the paper with some final observations.

Remarks on the notation conclude this section. Let $\mathbb{R}^{n\times n}_{sym}$, $n \in \mathbb{N}$, denote the set of all real symmetric $n \times n$ matrices, $\tau\colon \beta = \sum_{i,j=1}^{n} \tau_{ij}\beta_{ij} = \mathrm{tr}(\tau^T\beta)$ represents the scalar product in $\mathbb{R}^{n\times n}$, and $|\tau|$ the corresponding norm. Given a definite positive matrix $\mathbb{A}$, $|\tau|_{\mathbb{A}} := (\tau\colon \mathbb{A}\tau)^{1/2}$ denotes a norm equivalent to $|\tau|$. Given $u, v \in \mathbb{R}^m$, with $\mathbb{R}^m$ standing for either space of vectors or matrices, the symbol $u\cdot v$ denotes the inner product of the two elements of $\mathbb{R}^m$. Let Ω be a bounded, open connected set in $\mathbb{R}^d$, for $d = 2, 3$ with a Lipschitz boundary $\partial\Omega$, the Sobolev space $H^1(\Omega;\mathbb{R}^{n\times m})$ and the Lebesgue space $L^2(\Omega;\mathbb{R}^{n\times m})$ with $n, m \in \mathbb{N}$ are defined in the usual way. The space $L^2(\Omega;\mathbb{R}^n)$ is assumed equipped with the inner product $(\cdot,\cdot)_{L^2(\Omega;\mathbb{R}^n)}$ whereas for $u, v \in H^1(\Omega;\mathbb{R}^n)$ there holds $(u, v)_{H^1(\Omega;\mathbb{R}^n)} := (u, v)_{L^2(\Omega;\mathbb{R}^n)} + (Du, Dv)_{L^2(\Omega;\mathbb{R}^{n\times d})}$. Given $\tau \in L^2(\Omega;\mathbb{R}^{n\times n})$, set $|||\tau|||_{\mathbb{A};\Omega} := (\int_\Omega |\tau|^2_{\mathbb{A}} dx)^{1/2} = (\tau, \mathbb{A}\tau)^{1/2}_{L^2(\Omega;\mathbb{R}^{n\times n})}$.

2. Setting of the problem

In this section we formulate the primal problem of associative rate-indipendent plasticity in small strain. We focus on one typical step of an incremental procedure applied to the solution of the evolution of the elastoplastic body.

2.1. **The strong and primal weak formulation.** Let $\Omega \subset \mathbb{R}^d$, $d = 2$, 3, represent the reference configuration of an elastoplastic body with boundary $\partial\Omega = \Gamma_D \cup \Gamma_N$, and ν the outer unit normal. The boundary $\partial\Omega$ is split into a closed Dirichlet part Γ_D with positive surface measure and into a Neumann part $\Gamma_N := \partial\Omega\backslash\Gamma_D$ (possibly empty) where traction forces are prescribed by $g \in L^2(\Gamma_N;\mathbb{R}^d)$. The strong form of equilibrium conditions states that the stress field $\sigma \in L^2(\Omega;\mathbb{R}^{d\times d}_{sym})$ satisfies

$$\mathrm{div}\,\sigma + f = 0 \text{ in } \Omega, \quad \sigma\nu = g \text{ on } \Gamma_N\,, \tag{2.1}$$

where $f \in L^2(\Omega;\mathbb{R}^d)$ denotes the applied volume force. We suppose, for sake of simplicity, homogeneous geometric boundary conditions for the displacement field u and introduce the following space of admissible displacements

$$V := \{v \in H^1(\Omega;\mathbb{R}^d) :\ v = 0 \text{ on } \Gamma_D\},$$

equipped with the $H^1(\Omega;\mathbb{R}^d)$–norm and boundary values to be interpreted in the sense of the trace theorem; V is a closed subspace of $H^1(\Omega;\mathbb{R}^d)$.
Assuming the linear strain

$$\varepsilon(u) := \mathrm{sym}(Du) = 1/2(Du + Du^T)$$

split into an elastic e and plastic part p, i.e.

$$\varepsilon(u) = e + p\,,$$

and introduced additional internal variables $\alpha \in \mathbb{R}^m$, the linear elastic law is defined by the isotropic elasticity tensor $\mathbb{C}$ such that

$$\mathbb{C}\delta = 2\mu\delta + \lambda\,\mathrm{tr}\,\delta\, I \quad \text{for } \delta \in \mathbb{R}^{d\times d}_{sym}\,,$$

and λ, μ being the Lamé material constants. The elasticity tensor $\mathbb{C}$ is elliptic in the sense of

$$\kappa|\delta|^2 \le \mathbb{C}\delta\colon \delta \quad \text{with } \kappa = \frac{1}{d\lambda + 2\mu}\,. \tag{2.2}$$

Denoting by $A \in \mathbb{R}^m$ the thermodynamic forces conjugate to α, we assume the hardening law in the form $A = \mathbb{H}\alpha$ with the hardening moduli $\mathbb{H}$ such that $\mathbb{H}\alpha \cdot \alpha > h|\alpha|^2$ for $\alpha \neq 0$ and $h > 0$. Upon the condition that $\mathbb{C}$ and $\mathbb{H}$ are piecewise constant over Ω, we set

$$\Lambda = \min_{x\in\Omega} \kappa(x) \quad \text{and} \quad \mathsf{h} = \min_{x\in\Omega} h(x)\,. \tag{2.3}$$

Rate-independent plasticity models are specified by assigning the dissipation function $j = j(p, \alpha)$ as lowersemicontinuous (hereafter abreviated as lsc), convex, and positively homogeneous of degree one, resulting in its non differentiability at the point $(0, 0)$. Without loss of generality, considering initial conditions equal to zero in the time discrete form of the evolution law, the latter is expressed as

$$(p, \alpha) \in \partial j^*(\sigma, A) \quad \text{or in the dual form} \quad (\sigma, A) \in \partial j(p, \alpha)\,, \tag{2.4}$$

with j^* Legendre-Fenchel transform of j, and ∂f subdifferential of the convex function f [22].

Remark 2.1. *Let $\mathbb{E} := \partial j(0, 0) \subset \mathbb{R}^{d\times d} \times \mathbb{R}^m$, which is convex and closed, then duality theory shows that j is the Legendre-Fenchel transform of the indicator function of $\mathbb{E}$ and is referred to as support function of $\mathbb{E}$. The set $\mathbb{E}$ is called elastic domain and defines the set of admissible generalised stresses (σ, A)* [25].

The primal problem of elastoplasticity of [32] assumes (u, p, α) as primary variables. Choosing $Q := \{q \in L^2(\Omega; \mathbb{R}^{d\times d}_{sym}) : \operatorname{tr} q = 0 \text{ a.e. in } \Omega\}$ as space of the plastic strains and $M := L^2(\Omega; \mathbb{R}^m)$ as space of the internal variables, we define the Hilbert space $\mathcal{H} := V \times Q \times M$ equipped with the inner product

$$(w, z)_{\mathcal{H}} = (u, v)_{H^1(\Omega;\mathbb{R}^d)} + (p, q)_{L^2(\Omega;\mathbb{R}^{d\times d})} + (\alpha, \beta)_{L^2(\Omega;\mathbb{R}^m)}$$

for $w := (u, p, \alpha) \in \mathcal{H}$, $z := (v, q, \beta) \in \mathcal{H}$ and norm $\|\cdot\|_{\mathcal{H}}$.

Let $\sigma := \mathbb{C}(\varepsilon(u) - p)$ and introduce

$$a : \mathcal{H} \times \mathcal{H} \to \mathbb{R}, \qquad a(w, z) := (\sigma, \varepsilon(v) - q)_{L^2(\Omega;\mathbb{R}^{d\times d})} + (\mathbb{H}\alpha, \beta)_{L^2(\Omega;\mathbb{R}^m)} \tag{2.5}$$

$$b : \mathcal{H} \to \mathbb{R}, \qquad b(z) := (f, v)_{L^2(\Omega;\mathbb{R}^d)} + \int_{\Gamma_N} g \cdot v \, ds \tag{2.6}$$

$$\psi : \mathcal{H} \to \mathbb{R}, \qquad \psi(z) := \int_\Omega j(q, \beta)\, dx\,. \tag{2.7}$$

The weak form of the primal problem is then given by the following variational inequality [21], usually referred to as of second kind [20]: Given $b \in \mathcal{H}^*$, the dual of $\mathcal{H}$, find $w = (u, p, \alpha) \in \mathcal{H}$ such that there holds

$$b(z - w) \le a(w,\, z - w) + \psi(z) - \psi(w) \quad \text{for all } z \in \mathcal{H}\,. \tag{2.8}$$

The functional b is linear and bounded on $\mathcal{H}$; ψ is convex, lsc, positively homogeneous on $\mathcal{H}$, and non differentiable, whereas the bilinear form a is symmetric and continuous on $\mathcal{H}$. For ease of the presentation, we consider plasticity models such that a is elliptic all over the space $\mathcal{H}$ with constant K, i.e.

$$K\|z\|^2_{\mathcal{H}} \le a(z, z) \quad \text{for every } z \in \mathcal{H}\,. \tag{2.9}$$

Under the above assumptions, (2.8) has solution and is unique. The reader is referred to [21, page 168] for a discussion on the more general case with the ellipticity holding only on a closed convex cone of $\mathcal{H}$.

By taking $q = p$ in (2.8) and choosing once $v = u + r$ and then $v = u - r$ for every $r \in V$, we deduce the weak form of the equilibrium equations

$$(\sigma, \varepsilon(v))_{L^2(\Omega;\mathbb{R}^{d\times d})} = b(v) \text{ for every } v \in V\,. \tag{2.10}$$

Let the energy functional $J : \mathcal{H} \mapsto \mathbb{R}$ be defined as

$$J(z) = \frac{1}{2}a(z,\, z) - b(z) + \psi(z)\,. \tag{2.11}$$

It is a standard result of optimization theory [20] showing that the variational inequality (2.8) is equivalent to the minimization problem

$$w = \arg\min_{z\in\mathcal{H}}\ J(z)\,, \tag{2.12}$$

and to the stationariety condition

$$0 \in \partial J(w)\,. \tag{2.13}$$

Since $J(\cdot)$ is sum of the lsc and uniformly convex function $\phi(\cdot) := 1/2a(\cdot,\cdot) - b(\cdot)$ and of the lsc and convex function $\psi(\cdot)$, then J itself is lsc and uniformly convex, i.e., with the constant K from (2.9), there holds for every $z, y \in \mathcal{H}$

$$J(z) \geq J(y) + \langle s, z - y\rangle + \frac{K}{2}\|z - y\|^2_{\mathcal{H}} \quad \text{for every } s \in \partial J(y)\,. \tag{2.14}$$

Proof of (2.14). Under the above assumptions on $\phi(\cdot)$ and $\psi(\cdot)$, with $\phi(\cdot)$ being continuous on $\mathcal{H}$ in particular, the subdifferential calculus rule [19, page 26] gives

$$\partial(\phi + \psi) = \partial\phi + \partial\psi\,.$$

As a result, for any $s \in \partial J(y)$ there holds

$$J(z) - J(y) - \langle s, z - y\rangle = \phi(z) - \phi(y) - \langle s_\phi, z - y\rangle + \psi(z) - \psi(y) - \langle s_\psi, z - y\rangle \tag{2.15}$$

with $s_\phi \in \partial\phi(y)$ and $s_\psi \in \partial\psi(y)$. Since ψ is convex and ϕ is differentiable, for every $z \in \mathcal{H}$, there holds

$$\psi(z) - \psi(y) - \langle s_\psi, z - y\rangle \geq 0 \quad \text{and} \quad \langle s_\phi, z - y\rangle = a(y, z - y) - b(z - y)\,.$$

As a result, (2.15) is bounded from below by

$$\frac{1}{2}a(z, z) - \frac{1}{2}a(y, y) - a(y, z - y) = \frac{1}{2}a(z - y, z - y)\,.$$

Accounting for (2.9), one obtains (2.14). □

3. Examples of rate-independent plasticity models

This section introduces several rate-independent plasticity models. For each of them we give the expression of the dissipation functional and specify the dependence of the constant K from (2.9).

3.1. **Plasticity with combined isotropic/kinematic hardening.** Let $m = 1 + d(d+1)/2$, identify $\mathbb{R}^m \equiv \mathbb{R}^{d\times d} \times \mathbb{R}$, and assume $\alpha = (\xi, a)$ where ξ, generally taken

to be the plastic strain p as in this case, is the kinematic–type internal variable conjugate of the back stress tensor χ, and a is the accumulated plastic strain with R as its dual variable. Introduce the elastic domain

$$\mathbb{E} := \{(\sigma, \chi, R) \in \mathbb{R}^{d\times d}_{sym} \times \mathbb{R}^{d\times d} \times \mathbb{R} \,|\, \phi(\sigma, \chi, R) \leq 0, \quad R \geq 0\}, \tag{3.1}$$

where $\phi(\sigma, \chi, R)$ is the continuous and convex von-Mises yield function

$$\Phi(\sigma, \chi, R) := |\operatorname{dev}(\sigma - \chi)| - (\sigma_y + R), \tag{3.2}$$

and $\sigma_y > 0$ is a material constant referred to as the yield stress. The support function of $\mathbb{E}$ is then defined as follows

$$j(q, a) = \begin{cases} \sigma_y |q| & \text{if } |q| - a \leq 0 \text{ and } \operatorname{tr} q = 0, \\ \infty & \text{otherwise}. \end{cases}$$

Also, we assume a linear hardening state law in the form

$$\chi = \mathbb{H}p \quad \text{and} \quad R = Ha\,,$$

with $\mathbb{H}$ definite positive and such that $\mathbb{H}\delta\colon \delta \geq h|\delta|^2$, H the isotropic hardening modulus, and we set $\mathsf{H} = \min_{x\in\Omega} H(x) > 0$. Then, the bounds (2.3), and Young inequality show, with $d \in (2\Lambda/(2\Lambda + \mathsf{h}),\, 1)$ and $K = \min\{C_{korn}\Lambda(1-d), \Lambda(1 - 1/d) + \mathsf{h}, \mathsf{H}\}$[21], that

$$\begin{aligned} a(z; z) &\geq \Lambda\|\varepsilon(v) - q\|^2_{L^2(\Omega;\mathbb{R}^{d\times d})} + \mathsf{h}\|q\|^2_{L^2(\Omega;\mathbb{R}^{d\times d})} + \mathsf{H}\|a\|^2_{L^2(\Omega;\mathbb{R})} \\ &\geq \Lambda(1-d)\|\varepsilon(v)\|^2_{L^2(\Omega;\mathbb{R}^{d\times d})} + (\Lambda(1 - \frac{1}{d}) + \mathsf{h})\|q\|^2_{L^2(\Omega;\mathbb{R}^{d\times d})} + \mathsf{H}\|a\|^2_{L^2(\Omega;\mathbb{R})} \\ &\geq K(\|v\|_{H^1(\Omega;\mathbb{R}^d)} + \|q\|^2_{L^2(\Omega;\mathbb{R}^{d\times d})} + \|a\|^2_{L^2(\Omega;\mathbb{R})})\,. \end{aligned} \tag{3.3}$$

3.2. **Kinematic hardening.** As special case of the model described in the previous section, we assume as single internal variable ξ the plastic strain p with the conjugate back stress χ. Considering, as before, Von Mises plasticity with

$$\mathbb{E} := \{(\sigma, \chi) \in \mathbb{R}^{d\times d}_{sym} \times \mathbb{R}^{d\times d} \,|\, \operatorname{dev}(\sigma - \chi) - \sigma_y \leq 0\},$$

one obtains for the dissipation potential the following expression

$$j(q) = \sigma_y |q| \quad \text{for } \operatorname{tr} q = 0\,. \tag{3.4}$$

Following the same arguments as in the previous model, one easily constate the ellipticity of $a(z, z)$ all over the space $\mathcal{H} = V \times Q$ with $K = \min\{C_{korn}\Lambda(1 - d), \Lambda(1 - 1/d) + h\}$ for $d \in (2\Lambda/(2\Lambda + h),\, 1)$.

3.3. **Multiyield plasticity.** Multiyield surface plasticity models are often used to model nonlinear kinematic hardening by a set of nested surfaces, each of which only exhibits linear hardening [30], and represent the adequate constitutive framework for e.g. single crystal plasticity [24, 34]. The corresponding rheological model is displayed in Figure 1.
The plastic component is assumed to be given by

$$p = \sum_{r\in I} p_r \text{ with } I := \{1, 2, ..., M\}, \quad p_r \in Q\,.$$

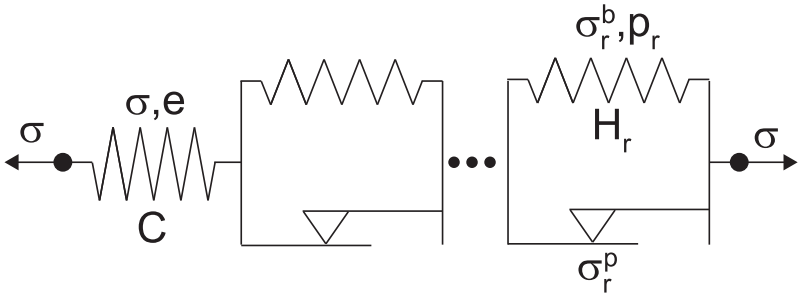

FIGURE 1. Multisurface plasticity: Rheological model

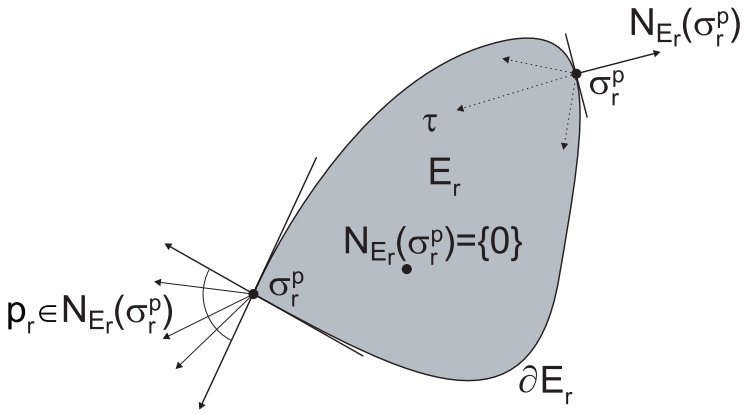

FIGURE 2. Multisurface plasticity: Evolution law for the plastic strain p_r associated with the hardening mechanism $r \in I$. $N_{\mathbb{E}_r}$ denotes the normal cone to $\mathbb{E}_r$ [22]

Correspondently, for the stress $\sigma = \mathbb{C}e$ is assumed the decomposition $\sigma = \sigma_r^p + \sigma_r^b$ depending on the hardening mechanism r that is activated. The position of the set $\mathbb{E}_r$ of the admissible stresses $\sigma_r^p = \sigma - \sigma_r^b$ associated with the hardening mechanism r is defined by the stress σ_r^b related to p_r by the linear hardening law $\sigma_r^p = \mathbb{H}_r p_r$, with $\mathbb{H}_r$ a positive definite tensor of the hardening moduli such that $\mathbb{H}_r\delta\colon \delta > h_{min,r}|\delta|^2$. The plastic flow of each p_r is described by the associative flow rule (see Figure 2)

$$\sigma_r^p \in \mathbb{E}_r, \quad p_r\colon (\tau_r - \sigma_r^p) \leq 0 \quad \text{for all } \tau_r \in \mathbb{E}_r,\ r \in I.$$

For single yield surface, σ^b is referred to as back stress and one obtains the model of Melan-Prager of linear kinematic hardening described in Scetion 3.2. In the applications of this paper, each yield surface is of Von-Mises type, with σ_y^r value of the treshold for yielding with the mechanism r, i.e. the corresponding set of admissible stresses is defined as follows

$$\mathbb{E}_r = \{\tau \in \mathbb{R}^{d\times d}_{sym} : |\operatorname{dev}\tau| - \sigma_y^r \leq 0\},$$

with support function given by equation (3.4), i.e.,

$$j_r(q) = \sigma_y^r |q| \text{ with } \operatorname{tr} q = 0\,. \tag{3.5}$$

The model is transformed into the primary form of plasticity in [3] with $w = (u, (p_r)_{r\in I}) \in \mathcal{H} := V \times \prod_{r\in I} Q$, and considering the following definition of the bilinear form

$$a(w, z) := (\sigma, \varepsilon(v) - q)_{L^2(\Omega;\mathbb{R}^{d\times d})} + \sum_{r\in I} (\mathbb{H}_r p_r, q_r)_{L^2(\Omega;\mathbb{R}^{d\times d})}\,,$$

and of the convex functional

$$\psi(z) := \sum_{r\in I} \int_\Omega \sigma_r^y |q_r|\, dx\,.$$

In [3], the ellipticity of a is shown to hold over $\mathcal{H}$ with

$$K = k \min\{\lambda_{min}, \mathsf{h}_{min,1}, \ldots, \mathsf{h}_{min,\#I}\} \min\{1, C_{Korn}\}\,,$$

where $k > 0$ depends on the cardinality, $\#I$, of I and C_{Korn} is the constant in the Korn's first inequality.

3.4. **Perfect plasticity.** The model of perfect plasticity corresponds to the case of absence of hardening. Next, we recall some properties that will be useful in the analysis of Section 6.4. Using the elastic law in the primal form of the evolution law (2.4), one obtains for given ε

$$0 \le (\varepsilon - \mathbb{C}^{-1}\sigma) \colon (\sigma - \tau) \quad \text{for each } \tau \in \mathbb{E}. \tag{3.6}$$

By rearranging the terms in (3.6) as follows

$$\mathbb{C}^{-1}\sigma \colon (\sigma - \tau) \le \varepsilon \colon (\sigma - \tau) \quad \text{for each } \tau \in \mathbb{E}\,, \tag{3.7}$$

and using Von Mises plasticity, equation (3.7) defines $\sigma = \sigma(\varepsilon)$ as [15]

$$\sigma = (\lambda + \frac{2\mu}{d}) \operatorname{tr}(\varepsilon)\mathbb{I} + 2\mu \digamma(|\operatorname{dev}\varepsilon|) \operatorname{dev}\varepsilon\,,$$

with $\digamma(x) = 1 - max\{0, 1 - \frac{\sigma_y}{2\mu x}\}$. The mapping $\varepsilon \mapsto \sigma$ is monotone and Lipschitz continuous with $L = 1/\kappa$, i.e., there holds

$$|\sigma(\varepsilon_1) - \sigma(\varepsilon_2)| \le L|\varepsilon_1 - \varepsilon_2|\,.$$

Given the following strain energy function

$$W(\varepsilon) := \frac{1}{2}\varepsilon \colon \mathbb{C}\varepsilon - \frac{1}{4\mu}\max\{0, |\operatorname{dev}\mathbb{C}\varepsilon| - \sigma_y\}^2\,,$$

one can verify

$$\sigma = \frac{DW(\varepsilon)}{D\varepsilon}\,.$$

Hence, W is $C^1(\mathbb{R}^{d\times d}_{sym})$ with Lipschitz derivative.

4. The SOLVE & ESTIMATE step in AFEM

In this section we describe the steps `SOLVE` and `ESTIMATE` of (1.1). We first establish a two side bounds on the error of the energy, valid for any internal approximation

to the variational inequality, which is then specialized to the finite element approximations considered in the paper. The section concludes with an edge-residual based a posteriori error estimate and proof of its reliability.

4.1. **Internal approximation.** Internal discrete approximations to (2.8) are obtained by solving (2.8) over a finite dimensional subspace $\mathcal{H}_h$ of $\mathcal{H}$. The discrete problem then consists in finding $w_h = (u_h, p_h, \alpha_h) \in \mathcal{H}_h$ such that

$$b(z_h - w_h) \leq a(w_h,\, z_h - w_h) + \psi(z_h) - \psi(w_h) \quad \text{for all } z_h \in \mathcal{H}_h, \tag{4.1}$$

which is also equivalent to the following minimization problem

$$w_h = \arg\min_{z_h \in \mathcal{H}_h} \; J(z_h)\,. \tag{4.2}$$

Let $\sigma = \mathbb{C}(\varepsilon(u) - p)$ be the continuous stress field corresponding to $w = (u, p, \alpha) \in \mathcal{H}$ solution of (2.8) and $\sigma_h = \mathbb{C}(\varepsilon(u_h) - p_h)$ the discrete stress field associated with $w_h = (u_h, p_h, \alpha_h) \in \mathcal{H}_h$ solution of (4.1). Then we have the following bounds on the error of the energies.

$$\frac{1}{2}|||\sigma - \sigma_h|||^2_{\mathbb{C}^{-1};\Omega} \leq J(w_h) - J(w)\,; \tag{4.3}$$

$$J(w_h) - J(w) \leq \min_{z_h \in \mathcal{H}_h} a(w_h, z_h - w) - b(z_h - w) + \psi(z_h) - \psi(w)\,. \tag{4.4}$$

Proof of (4.3). From (4.1) with $z = w_h$, since $\mathcal{H}_h \subseteq \mathcal{H}$, after some rearrangements one obtains

$$\frac{1}{2}a(w - w_h, w - w_h) \leq J(w_h) - J(w)\,.$$

Expressing $a(x, y)$ from (2.5) in terms of σ_h and σ finally yields (4.3).

Proof of (4.4). Using the expression of J from (2.11), simple rearrangements show

$$J(w_h) - J(w) = \frac{1}{2}a(w_h + w, w_h - w) - b(w_h - w) + \psi(w_h) - \psi(w). \tag{4.5}$$

Since $1/2a(w_h - w, w_h - w) > 0$, (4.5) is bounded from above by the term

$$a(w_h, w_h - w) - b(w_h - w) + \psi(w_h) - \psi(w)\,. \tag{4.6}$$

For every z_h, (4.6) is also equal to

$$a(w_h, w_h - z_h) - b(w_h - z_h) + \psi(w_h) - \psi(z_h) + a(w_h, z_h - w) - b(z_h - w) + \psi(z_h) - \psi(w)$$

thus, accounting for (4.1), one obtains (4.4). □

4.2. **SOLVE: Space discretization and the finite element method.** For approximating (2.8) by the finite element method, we introduce a regular triangulation $\mathcal{T}$ of $\bar{\Omega} \subset \mathbb{R}^d$ in the sense of Ciarlet [16, 2] in closed triangles such that $\bigcup_{T \in \mathcal{T}} K = \bar{\Omega}$, two distinct elements T and T' in $\mathcal{T}$ are either disjoint, or share the common edge E, or a common vertex, that is, hanging nodes are not allowed. Let $\mathcal{E}$ denote the set of all edges in $\mathcal{T}$, $\mathcal{N}$ the set of nodes in $\mathcal{T}$ and $\mathcal{K}$ the subset of free nodes, i.e. the set of nodes that do not belong to Γ_D. The set of interior edges of Ω are denoted by $\mathcal{E}(\Omega)$, the set of edges of the element T by $\mathcal{E}(T)$, whereas those that belong to the Dirichlet and Neumann boundary are denoted by $\mathcal{E}(\Gamma_D)$ and $\mathcal{E}(\Gamma_N)$, respectively. Also, we denote by ω_E the patch of elements having in common the edge E. We

use the symbols m_E and m_T for the midpoint of the edge $E \in \mathcal{E}$ and of the element $T \in \mathcal{T}$, respectively. Given any edge $E \in \mathcal{E}$ we assign one fixed unit normal ν_E; for $E \in \mathcal{E}(\Gamma_D) \cup \mathcal{E}(\Gamma_N)$ we choose $\nu_E = \nu$. In relation to ν_E we then define the elements $T_+ \in \mathcal{T}$ and $T_- \in \mathcal{T}$, with $E \subseteq \partial T_- \cap \partial T_+$, depicted in Figure 3.

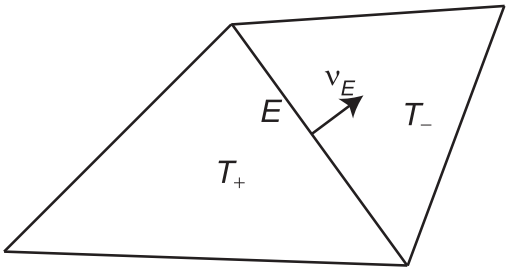

FIGURE 3. Definition of the finite element domains T_+ and T_- in relation to ν_E

Furthermore, given $E \in \mathcal{E}(\Omega)$ with unit normal ν_E and v a vector field defined in Ω, we denote by $[v]_E$ the jump of v across E in the direction ν_E, i.e.

$$[v]_E(x) = v|_{T_+}(x) - v|_{T_-}(x) \quad \text{for } x \in E \text{ and } E \subseteq \partial T_- \cap \partial T_+.$$

For any subset ω (patch, triangle, or edge), $\mathcal{K}(\omega)$ denotes the set of free nodes that belong to ω, whereas $P_k(\omega; \mathbb{R}^m)$ is the vector space of all algebraic polynomials with values in $\mathbb{R}^d$ for $m = d$ and in $\mathbb{R}^{d\times d}$ for $m = d \times d$, defined on ω of total degree at most $k \in \mathbb{N}$. Then,

$$P_k(\mathcal{T}; \mathbb{R}^m) := \{v_h \in L^\infty(\Omega; \mathbb{R}^m) : \forall T \in \mathcal{T},\, v_h|_T \in P_k(T; \mathbb{R}^m)\}$$

represent the set of piecewise polynomials of degree at most k where piecewise is with respect to the shape-regular triangulation $\mathcal{T}$; in general, the functions in $P_k(\mathcal{T}; \mathbb{R}^d)$ are discontinuous.

For all the aforementioned definitions, whenever necessary, we will adopt the subscript ℓ to mean that they refer to the triangulation $\mathcal{T}_\ell$ obtained after ℓ refinements. For instance, let ω_ℓ be a patch of elements of $\mathcal{T}_\ell$, $\mathcal{K}_{\ell+1}(\mathring{\omega}_\ell)$ denotes the set of free nodes in $\mathcal{T}_{\ell+1}$ that belong to the interior of ω_ℓ.

The conforming finite element approximation of (2.8) is next obtained by considering continuous piecewise affine functions

$$P_1 := P_1(\mathcal{T}; \mathbb{R}^d) \cap C(\overline{\Omega}; \mathbb{R}^d) \quad \text{and} \quad V_\ell := P_1 \cap V,$$

as approximation for the displacement field u, piecewise constant functions with zero trace

$$Q_0 := \{q \in P_0(\mathcal{T}; \mathbb{R}^d) : \operatorname{tr}(q) = 0\}$$

as approximation of the plastic strain p, and the space of piecewise constant functions

$$P_0 := P_0(\mathcal{T}; \mathbb{R}^d)$$

for the approximation of the internal variables α.

For future derivations, we need to know that there exists a quasi-interpolation operator $\mathcal{J} : V \mapsto V_\ell$ as in [6, 11] with the following properties for all $\varphi \in V$ and

$f \in L^2(\Omega;\mathbb{R}^d)$

$$
\begin{aligned}
&\|\nabla \mathcal{J}\varphi\|_{L^2(\Omega;\mathbb{R}^{d\times d})} + \|h_{\mathcal{T}}^{-1}(\varphi - \mathcal{J}\varphi)\|_{L^2(\Omega;\mathbb{R}^d)} \le C\|\nabla\varphi\|_{L^2(\Omega;\mathbb{R}^{d\times d})}\,,\\
&\|h_{\mathcal{E}}^{-1/2}(\varphi - \mathcal{J}\varphi)\|_{L^2(\Gamma_N;\mathbb{R}^d)} \le C\|\nabla\varphi\|_{L^2(\Omega;\mathbb{R}^{d\times d})}\,,\\
&\int_\Omega f\cdot(\varphi - \mathcal{J}\varphi)\,dx \le C\|\nabla\varphi\|_{L^2(\Omega;\mathbb{R}^{d\times d})}\Big(\sum_{z\in\mathcal{K}} h_z^2 \min_{a\in\mathbb{R}^d}\|f-a\|^2_{L^2(\Omega_z;\mathbb{R}^d)}\Big)^{1/2}\,,
\end{aligned}
\tag{4.7}
$$

where the constant C depends only on the shape regularity of the mesh $\mathcal{T}$. In (4.7), $h_{\mathcal{T}}$ and $h_{\mathcal{E}}$ denote the local mesh-sizes, with $h_{\mathcal{T}}|_T := h_T := \operatorname{diam}(T)$ for $T \in \mathcal{T}$, and $h_{\mathcal{E}}|_E := \operatorname{diam}(E)$, whereas $h_z := \operatorname{diam}(\Omega_z)$ defines the patch-size for each node $z \in \mathcal{K}$. As for the definition of Ω_z for $z \in \mathcal{K}$, for each fixed node $z \in \mathcal{N}\setminus\mathcal{K}$ we choose a free node $\zeta(z) \in \mathcal{K}$ and let $\zeta(z) = z$ if $z \in \mathcal{K}$. In this way we realize a partition of $\mathcal{N}$ in classes $I(z) := \{z \in \mathcal{N} : \zeta(z) = z\}$. Let $(\varphi_z)_{z\in\mathcal{N}}$ denote the nodal-shape basis of the space P_1, we then set

$$
\psi_z := \sum_{\zeta\in I(z)} \varphi_z \quad\text{and}\quad \Omega_z := \overline{\{x\in\Omega : \psi_z(x) > 0\}}\,,
\tag{4.8}
$$

with $\bar\omega$ the closure of ω. Given $z \in \mathcal{N}$, let

$$
\omega_z := \overline{\{x\in\Omega : \varphi_z(x) > 0\}} = \overline{\{T\in\mathcal{T} : z\in T\}}\,,
$$

then for $z \in \mathcal{K}$,

$$
\Omega_z = \bigcup_{\xi\in I(z)} \omega_\xi\,.
$$

See Figure 4 for an illustration of ω_z and Ω_z. The functions $(\psi_z)_{z\in\mathcal{K}}$ realize a partition of unity on Ω and are used to define $\mathcal{J}$. For further details on the construction of $\mathcal{J}$ we refer to [6].

We conclude this section by highlighting some properties of the finite element solution. Assuming $\mathcal{H}_\ell := V_\ell \times Q_0 \times P_0 \subset \mathcal{H}$ as finite element space, and under the additional assumption that $\mathbb{C}$ and $\mathbb{H}$ are piecewise constant with respect to $\mathcal{T}_\ell$, we have

$$
J(w_\ell) - J(w) \le (\sigma_\ell - \sigma, \varepsilon(v_\ell - u))_{L^2(\Omega;\mathbb{R}^{d\times d})} \text{ for all } v_\ell \in V_\ell\,.
\tag{4.9}
$$

with $w \in \mathcal{H}$ and $w_\ell \in \mathcal{H}_\ell$ solution of (2.8) and (4.1), respectively.

Proof of (4.9). Given $w = (u, p, \alpha)$ solution of (2.8), consider $z_\ell = (v_\ell, q_\ell, \beta_\ell) \in \mathcal{H}_\ell$ with $(q_\ell, \beta_\ell)|_T := 1/|T| \int_T j(p,\alpha)\,dx$. Then Jensen's inequality gives

$$
j(q_\ell, \beta_\ell) \le \frac{1}{|T|}\int_T j(p,\alpha)\,dx,
$$

the integration over T and the definition of ψ from (2.7) yields

$$
\psi(z_\ell) \le \psi(w)\,.
\tag{4.10}
$$

In the remaining terms of $a(w_\ell, w - z_\ell)$ the differences $p - q_\ell$ and $\alpha - \beta_\ell$ have integral mean zero over each element. Hence, $(\sigma_\ell, p - q_\ell) = 0$ and $(\mathbb{H}\alpha_\ell, \alpha - \beta_\ell) = 0$ as $\mathbb{C}$ and $\mathbb{H}$ are piecewise constant with respect to $\mathcal{T}_0$, and $\sigma_\ell|_T$, $p_\ell|_T$, and $\alpha_\ell|_T$ are constant over each $T \in \mathcal{T}_\ell$. These arguments and (4.10) in (4.4) show finally (4.9). □

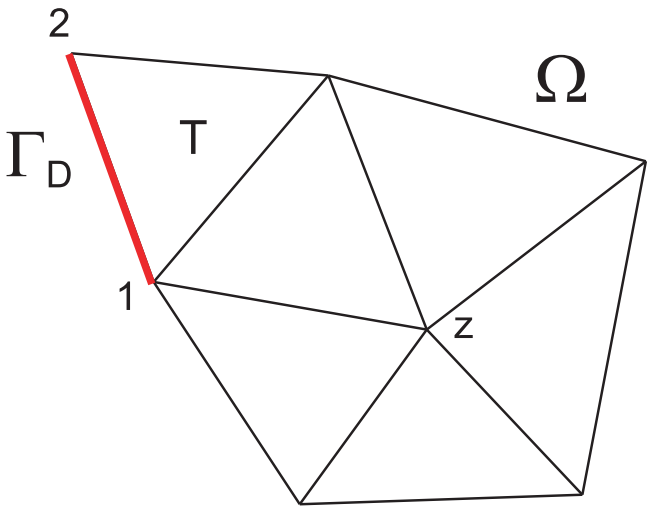

FIGURE 4. For the triangulation of Ω shown in Figure, by assigning the fixed node 1 to the free node z, it is $\Omega_z = \Omega$ whereas $\omega_z := \{T \in \mathcal{T} : z \in T\} = \Omega \setminus T$.

4.3. **Data oscillations.** For the volume load f and mesh $\mathcal{T}_\ell$, we define for $j \in \mathcal{K}_\ell$ the patchwise oscillations of f as follows [8],

$$\operatorname{osc}_\ell^2(f) := \sum_{j\in\mathcal{K}_\ell} \operatorname{osc}_{j,\ell}^2(f) \text{ with } \operatorname{osc}_{j,\ell}^2(f) = h_{j,\ell}^2 \, \|f - f_{j,\ell}\|^2_{L^2(\Omega_{j,\ell};\mathbb{R}^d)} \,. \tag{4.11}$$

Here $f_{j,\ell}$ is the L^2-projection of f onto the constant functions defined over $\Omega_{j,\ell}$, that is $f_{j,\ell} = 1/|\Omega_{j,\ell}| \int_{\Omega_{j,\ell}} f \, dx$ with $\Omega_{j,\ell}$ from (4.8). Whenever we need to point out the domain of definition, we will use the notations $\operatorname{osc}_{j,\ell}(f;\Omega_{j,\ell})$ for $\operatorname{osc}_{j,\ell}(f)$ and $\operatorname{osc}_\ell(f;\Omega)$ for $\operatorname{osc}_\ell(f)$. Furthermore, for $\mathcal{T}_{\ell+1}$ obtained as refinement of $\mathcal{T}_\ell$ we denote by $\operatorname{osc}_{\ell+1}(f;\Omega_{j,\ell})$ the oscillations on the node patches of $\mathcal{T}_{\ell+1}$ contained in the interior of $\Omega_{j,\ell}$, that is

$$\operatorname{osc}_{\ell+1}^2(f;\Omega_{j,\ell}) := \sum_{i\in\mathcal{K}_{\ell+1}(\mathring{\Omega}_{j,\ell})} \operatorname{osc}_{i,\ell+1}^2(f;\Omega_{i,\ell+1}) \,, \tag{4.12}$$

with $\mathcal{K}_{\ell+1}(\mathring{\Omega}_{j,\ell})$ defined in Section 4.2.
For the boundary tractions g on Γ_N we simply define

$$\operatorname{osc}_\ell^2(g) := \sum_{E\in\mathcal{E}(\Gamma_N)} \operatorname{osc}_{\ell,E}^2(g) \text{ with } \operatorname{osc}_{\ell,E}^2(g) := \|h_E^{1/2}(g - g_E)\|^2_{L^2(E;\mathbb{R}^d)} \,, \tag{4.13}$$

where $g_E := 1/h_E \int_E g \, ds$.

4.4. **ESTIMATE: A posteriori error estimator and its reliability.** For each $E \in \mathcal{E}_\ell$, let

$$\eta_\ell := (\sum_{E\in\mathcal{E}_\ell} \eta_E^2)^{1/2} \quad \text{with} \quad \eta_E^2 := \|h_E^{1/2} J_E\|^2_{L^2(E;\mathbb{R}^d)} \,, \tag{4.14}$$

and

$$J_E := \begin{cases} [\sigma_\ell \nu_E] & \text{if } E \in \mathcal{E}(\Omega), \\ 0 & \text{if } E \in \mathcal{E}(\Gamma_D), \\ g - \sigma_\ell \nu & \text{if } E \in \mathcal{E}(\Gamma_N). \end{cases} \tag{4.15}$$

Then there exists a positive constant C_{rel} depending on the Hook tensor $\mathbb{C}$, hardening moduli $\mathbb{H}$, and regularity of the mesh such that there holds

$$|||\sigma - \sigma_\ell|||_{\mathbb{C}^{-1};\Omega} \le C_{rel}(\eta_\ell + \operatorname{osc}_\ell(f)) \tag{4.16}$$

Proof of (4.16). Comparing (2.10) with the discrete counterpart shows that for $\mathcal{J}$ defined in Section 4.2 and for all $v \in V$, it is

$$(\sigma - \sigma_\ell, \varepsilon(\mathcal{J}(v)))_{L^2(\Omega;\mathbb{R}^{d\times d})} = 0\,. \tag{4.17}$$

Combining (4.3) and (4.4), accounting for (4.9) and (4.17), after some rearrangements and using the estimates (4.7) one obtains

$$\begin{aligned} \frac{1}{2}|||\sigma - \sigma_\ell|||^2_{\mathbb{C}^{-1};\Omega} &\le \sum_{T\in\mathcal{T}} \int_T f \cdot (e - \mathcal{J}e)\, dx + \sum_{E\in\mathcal{E}} \int_E J_E \cdot (e - \mathcal{J}e)\, ds \\ &\le C\|\nabla e\|_{L^2(\Omega;\mathbb{R}^{d\times d})} \Big((\sum_{z\in\mathcal{K}} \operatorname{osc}_z^2(f))^{1/2} + \big(\sum_{E\in\mathcal{E}} \|h_E^{1/2} J_E\|^2_{L^2(E;\mathbb{R}^d)}\big)^{1/2} \Big), \end{aligned}$$

where $e := u - u_\ell$ and C is the interpolation constant from (4.7). The Korn inequality $\|\nabla e\|_{L^2(\Omega;\mathbb{R}^{d\times d})} \le C_{Korn}\|\varepsilon(e)\|_{L^2(\Omega;\mathbb{R}^{d\times d})}$ with C_{Korn} depending on Ω and Γ_D, the bound $\|\varepsilon(e)\|_{L^2(\Omega;\mathbb{R}^{d\times d})} \le C_{\mathbb{HC}}\|\sigma - \sigma_\ell\|_{L^2(\Omega;\mathbb{R}^{d\times d})}$ from [23, 14] with $C_{\mathbb{HC}}$ depending on the hardening moduli and the Hook tensor, and the inequality

$$\|\sigma - \sigma_\ell\|_{L^2(\Omega;\mathbb{R}^{d\times d})} \le 1/\sqrt{\Lambda}|||\sigma - \sigma_\ell|||_{\mathbb{C}^{-1};\Omega}$$

from (2.3) proves (4.16) with $C_{rel} = 2CC_{Korn}C_{\mathbb{HC}}/\sqrt{\Lambda}$.

Remark 4.1. *Explicit expressions for the constant $C_{\mathbb{HC}}$ can be found in* [14]. *For single yield surface with linear kinematic hardening, one obtains $C_{\mathbb{HC}} = 1/(2\mu)+2/k$, with k the hardening moduli.*

5. The MARK & REFINE step in AFEM

This section presents the two basic ingredients of the adaptive algorithm (1.1): the step `MARK` and `REFINE`, and then concludes with an example of an adaptive algorithm.

5.1. MARK: Marking strategies for error and data oscillation reduction.

Error and data oscillation reduction depend crucially on the strategy used to select edges and node-patches to be refined. The idea is to give criteria that guarantee a fixed reduction rate independent on the refinement level. In this paper we consider the marking strategy introduced in [17] to enforce error reduction. Given $\Theta \in (0,1)$, we select a subset $\mathcal{M}_\ell$ of $\mathcal{E}_\ell$ in the current triangulation $\mathcal{T}_\ell$ with

$$\Theta\eta_\ell^2 \le \sum_{E\in\mathcal{M}_\ell} \eta_E^2\,. \tag{5.1}$$

For the control of data oscillations, following [27, 28], we consider criteria similar to (5.1). For the oscillations of f, given $\Theta_f \in]0, 1[$, we therefore select a set of nodes $\hat{\mathcal{K}}_\ell \subset \mathcal{K}_\ell$ such that for the associated patches there holds

$$\Theta_f \mathrm{osc}_\ell^2(f) \leq \sum_{z \in \hat{\mathcal{K}}_\ell} \mathrm{osc}_{\ell,z}^2(f)\,. \tag{5.2}$$

In a similar manner, for the oscillations of the Neumann boundary traction, we select a set $\hat{\mathcal{E}}_\ell(\Gamma_N) \subseteq \mathcal{E}_\ell(\Gamma_N)$ of edges $E \in \mathcal{E}_\ell(\Gamma_N)$ with

$$\Theta_g \mathrm{osc}_\ell^2(g) \leq \sum_{E \in \hat{\mathcal{E}}_\ell(\Gamma_N)} osc_{\ell,E}^2(g)\,. \tag{5.3}$$

5.2. **REFINE: Refinement rules and closure algorithm.** It is important that the triangles (marked for refinement) are divided according to some rules that insure that the angles remain bounded away from 0 and π. This is to avoid bad conditioning of the stiffness matrix and large growth of the interpolation error, respectively [26, 33]. With each triangle $T \in \mathcal{T}_\ell$ we therefore associate an edge $RE(T)$ referred to as the reference edge of T, which can be the longest edge [33] or the one defined as in Figure 5 according to how the element T is refined [7]. We then use the rule that if the edge $E \in T$ is marked, then one must mark also its reference edge $RE(T)$, and the type of refinement depends on the number of edges that are marked, if not specified otherwise by requiring `bisec5(T)`.

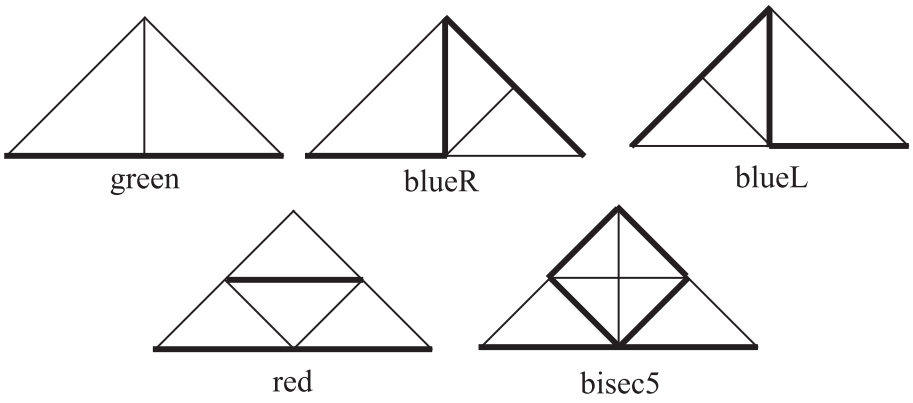

FIGURE 5. Type of refinement rules for the triangular element T. The bold line denotes the reference edge for the children elements after refinement of T.

Finally, we call closure algorithm the procedure that enlarges the set of marked edges so that using the above refinement rule we obtain a regular triangulation, i.e. without hanging nodes.

5.3. **Adaptive algorithm.** Given an initial triangulation $\mathcal{T}_0$ with $\mathbb{C}$ and $\mathbb{H}$ constant over each element $T \in \mathcal{T}_0$, we consider triangulations $\mathcal{T}_\ell$ built according to the following algorithm.

Algorithm 5.1.
Input a coarse shape-regular triangulation $\mathcal{T}_0$ of Ω into triangles with set of edges $\mathcal{E}_0$, $0 < \Theta < 1$, and repeat $(a) - (g)$.

(a) `SOLVE`*: Solve the nonlinear discrete problem,*

$$w_\ell = \underset{z_\ell \in \mathcal{H}_\ell}{arg\ min}\ J(z_\ell) \text{ and set } \sigma_\ell := \mathbb{C}(\varepsilon(u_\ell) - p_\ell)\,.$$

(b) `ESTIMATE`*: Given any $E \in \mathcal{E}_\ell$ with measure h_E, compute*

$$\eta_E^2 := h_E \int_E |J_E|^2\, ds \text{ for each } E \in \mathcal{E}_\ell \text{ and } \eta_\ell = (\sum_{E\in\mathcal{E}_\ell} \eta_E^2)^{1/2}\,.$$

(c) `MARK`*: Select a subset $\mathcal{M}_\ell$ of $\mathcal{E}_\ell$ in the current triangulation $\mathcal{T}_\ell$ with*

$$\Theta\eta_\ell^2 \le \sum_{E\in\mathcal{M}_\ell} \eta_E^2\,.$$

(d) `MARK`*: Control data oscillations $\mathrm{osc}_\ell(f)$ and $\mathrm{osc}_\ell(g)$ by selecting node- and edge-patches according to* (5.2) *and* (5.3)*, respectively.*

(e) `REFINE`*: Refine all the elements T with some edge in $\mathcal{M}_\ell$ with* `bisect5(T)` [27, 9]*; Red-refine the elements of the selected node- and edge-patches that have not already been refined with* `bisect5(T)`*.*

(f) *Run the closure algorithm with red-green-blue refinement* [40]*. Denote with $\mathcal{T}_{\ell+1}$ the resulting shape-regular triangulation with associated discrete space $\mathcal{H}_{\ell+1}$.*

(g) *Set $\ell := \ell + 1$ and go to* ***(a)****.*

Output discrete stress fields σ_0, σ_1, ...σ_ℓ, ... in $L^2(\Omega; \mathbb{R}^{d\times d}_{sym})$ as approximation to $\sigma = \mathbb{C}(\varepsilon(u) - p)$.

Remark 5.1. *Notice that the algorithm is the same as in linear elasticity, for the estimate η is related only to the norm of the residual in the equilibrium equations.*

6. Energy reduction, data oscillation reduction, and convergence of stresses

In this section we present the main results of the paper: energy reduction, data oscillation reduction, and the strong convergence of the stresses $(\sigma_\ell)_{\ell\in\mathbb{N}}$ produced by the Algorithm 5.1.

6.1. **Energy reduction.** With the energy J defined from (2.11) and $\delta_\ell := J(w_\ell) - J(w)$, the Algorithm 5.1 enforces a fixed rate reduction of the energy (up to control of data oscillations). This means that for the family of triangulations $\mathcal{T}_\ell$ generated by the Algorithm 5.1 there exist positive constants ρ_E, C with $\rho_E < 1$, depending on the regularity of the initial triangulation $\mathcal{T}_0$ and on the material parameters, such that

$$\delta_{\ell+1} \le \rho_E\delta_\ell + C(\mathrm{osc}_\ell^2(f) + osc_\ell^2(g)). \tag{6.1}$$

The proof of (6.1) relies on establishing first the following local discrete efficiency estimates with positive constants C_1, C_2, and C_M, with C_i, $i = 1, 2$ depending on the

mesh regularity and C_M in addition on the smallest egeinvalue of the Hook tensor $\mathbb{C}$.

$$(6.2)\quad \|h_E^{1/2}[\sigma_\ell \nu_E]\|_{L^2(E;\mathbb{R}^d)} \le C_M \||\sigma_\ell - \sigma_{\ell+1}|\|_{\mathbb{C}^{-1};\omega_E} + C_1 \min_{a\in\mathbb{R}^d} \|h_E(f-a)\|_{L^2(\omega_E;\mathbb{R}^d)}$$

$$(6.3)\quad \|h_E^{1/2}(g-\sigma_\ell \nu)\|_{L^2(E;\mathbb{R}^d)} \le C_M \||\sigma_\ell - \sigma_{\ell+1}|\|_{\mathbb{C}^{-1};\omega_E} + C_1 \min_{a\in\mathbb{R}^d} \|h_E(f-a)\|_{L^2(\omega_E;\mathbb{R}^d)}$$

$$+ C_2 \|h_E^{1/2}(g-g_E)\|_{L^2(E;\mathbb{R}^d)}\,.$$

This is possible provided that for the edge $E \in \mathcal{E}_\ell$ that is bisected, the elements $T \in \omega_E$ are refined with `bisect5(T)`.

Proof of (6.2). In the design of $\mathcal{T}_{\ell+1}$, the edge $E \in \mathcal{M}_\ell \cap \mathcal{E}(\Omega)$ is bisected with the creation of the node $m_E \in \mathcal{N}_{\ell+1}$ and of the inner nodes m_{T_-}, $m_{T_+} \in \mathcal{N}_{\ell+1}$ (see Figure 6(a)). We use the new scalar nodal basis functions ϕ_{m_E}, $\phi_{m_{T_+}}$, $\phi_{m_{T_-}}$ with

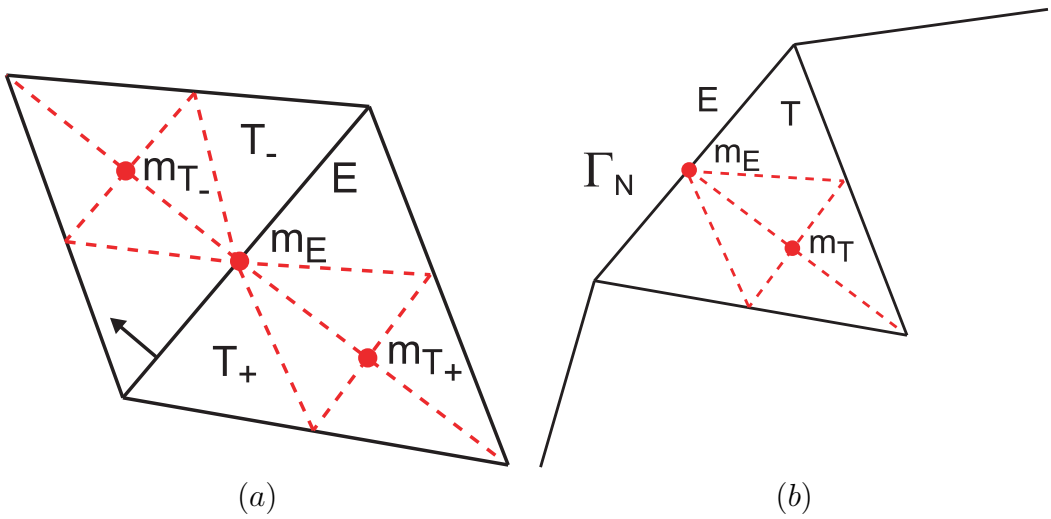

FIGURE 6. The inner node property for the elements T with the edge E in the set $\mathcal{M}_\ell$ defined by (5.1).

respect to $\mathcal{T}_{\ell+1}$ to define a function $b_E \in \operatorname{span}\{\phi_{m_E}, \phi_{m_{T_+}}, \phi_{m_{T_-}}\}$ with the following properties

$$(6.4)\quad \int_{T_+} b_E\,dx = 0\,,\quad \int_{T_-} b_E\,dx = 0\,,\quad \int_E b_E\,ds = \begin{cases} h_E/2 & \text{if } F = E\,,\\ 0 & \text{if } F \in \mathcal{E}_\ell \setminus \{E\}\,. \end{cases}$$

Such function b_E exists and has its support contained in

$$(6.5)\qquad \omega_E := \{T \in \mathcal{T}_\ell : E \in \mathcal{E}_\ell(T)\}\,.$$

Given an arbitrary integer k, there are constants C_1, C_2, which only depend on k and on the shape regularity of the triangulation, such that the following inequalities

$$\|b_E v\|_{H^1(\omega_E;\mathbb{R}^d)} \le c_1 h_E^{-1/2} \|v\|_{L^2(E;\mathbb{R}^d)}, \quad \|b_E v\|_{L^2(\omega_E;\mathbb{R}^d)} \le c_2 h_E^{1/2} \|v\|_{L^2(E;\mathbb{R}^d)},$$

$$\int_E b_E v \cdot v \, ds \le \|v\|^2_{L^2(E;\mathbb{R}^d)} \tag{6.6}$$

hold for all edges $E \in \mathcal{E}_\ell$, and all vector fields v with polynomials components of degree at most k [39].
Define $\psi_E := 2h_E[\sigma_\ell \nu_E] b_E \in V_{\ell+1}$ and since $[\sigma_\ell \nu_E]$ is constant along E one has

$$\|h_E^{1/2}[\sigma_\ell \nu_E]\|^2_{L^2(E;\mathbb{R}^d)} = \int_E [\sigma_\ell \nu_E] \cdot \psi_E \, ds. \tag{6.7}$$

Integrating by parts, observing that $\operatorname{div} \sigma_\ell|_T = 0$ for $T \in \mathcal{T}_\ell$, b_E vanishes over $\partial\omega_E$ and outside ω_E, and accounting for (2.10) stated over $V_{\ell+1}$ and (6.4), for any $a \in \mathbb{R}^d$ one arrives at

$$\int_E [\sigma_\ell \nu_E] \cdot \psi_E \, ds = \int_{\omega_E} \sigma_\ell : \varepsilon(\psi_E) \, dx = \int_{\omega_E} (\sigma_\ell - \sigma_{\ell+1}) : \varepsilon(\psi_E) \, dx + \int_{\omega_E} (f - a) \cdot \psi_E \, dx \,, \tag{6.8}$$

with no contribution from g, as $\psi_E = 0$ on Γ_N for $E \in \mathcal{E}(\Omega)$. Cauchy inequality, the definition of ψ_E, the estimates (6.6), and (2.3) yield the following bound for (6.8)

$$\|h_E^{1/2}[\sigma_\ell \nu_E]\|_{L^2(E;\mathbb{R}^d)} \left(\frac{2c_1}{\sqrt{\Lambda}} \|\sigma_\ell - \sigma_{\ell+1}\|_{\mathbb{C}^{-1};\omega_E} + 2c_2 \|h_E(f - a)\|_{L^2(\omega_E;\mathbb{R}^d)} \right). \tag{6.9}$$

for every $a \in \mathbb{R}^d$. Combining (6.9) with (6.7) concludes the proof of (6.2) with $C_M = \frac{2c_1}{\sqrt{\Lambda}}$ and $C_1 = 2c_2$. □

Proof of (6.3). For $E \in \mathcal{M}_\ell \cap \mathcal{E}(\Gamma_N)$, using ϕ_{m_E}, ϕ_{m_T} we define $b_E \in \operatorname{span}\{\phi_{m_E}, \phi_{m_T}\}$ upon the conditions

$$\int_T b_E \, dx = 0 \,, \quad \int_E b_E \, ds = \begin{cases} h_E/2 & \text{if } F = E \,, \\ 0 & \text{if } F \in \mathcal{E}_\ell \setminus \{E\} \,. \end{cases} \tag{6.10}$$

With b_E meeting the estimates (6.6) we set $\psi_E := 2h_E b_E (g_E - \sigma_\ell \nu)$ with g_E the mean integral value of g along $E \subset \Gamma_N$. Likewise the proof of (6.2), we write

$$\|h_E^{1/2}(g_E - \sigma_\ell \nu)\|^2_{L^2(E;\mathbb{R}^d)} = \int_E (g_E - \sigma_\ell \nu) \cdot \psi_E \, ds \,. \tag{6.11}$$

Integration by parts,(2.10) stated over $V_{\ell+1}$, and (6.10) yields for every $a \in \mathbb{R}^d$

$$\begin{aligned} \int_E (g_E - \sigma_\ell \nu) \cdot \psi_E \, ds = \int_{\omega_E} (\sigma_{\ell+1} - \sigma_\ell) : \varepsilon(\psi_E) \, dx + \int_E (g_E - g) \cdot \psi_E \, ds \\ - \int_{\omega_E} (f - a) \cdot \psi_E \, dx \,. \end{aligned} \tag{6.12}$$

Cauchy inequality, the estimates (6.6), combined with (6.11) give

(6.13)
$$\|h_E^{1/2}(g_E-\sigma_\ell\nu)\|_{L^2(E;\mathbb{R}^d)} \le 2c_1/\Lambda\|\sigma_\ell-\sigma_{\ell+1}\|_{\mathbb{C}^{-1};\omega_E} + 2c_2\|h_E(f-a)\|_{L^2(\omega_E;\mathbb{R}^d)} + 2\|h_E^{1/2}(g-g_E)\|_{L^2(E;\mathbb{R}^d)} \quad \text{for every } a\in\mathbb{R}^d\,.$$

Using (6.13) in the triangular inequality

(6.14) $$\|h_E^{1/2}(g-\sigma_\ell\nu)\|_{L^2(E;\mathbb{R}^d)} \le \|h_E^{1/2}(g-g_E)\|_{L^2(E;\mathbb{R}^d)} + \|h_E^{1/2}(g_E-\sigma_\ell\nu)\|_{L^2(E;\mathbb{R}^d)}\,,$$

proves finally (6.3) with $C_M=\frac{2c_1}{\sqrt{\Lambda}}$, $C_1=2c_2$, and $C_2=3$. □

Proof of (6.1). For the uniform convexity of J in $\mathcal{H}$ and since $0\in\partial J(w)$, one has

$$\frac{K}{2}\|w-w_\ell\|_{\mathcal{H}}^2 \le J(w_\ell)-J(w)\,. \tag{6.15}$$

From (4.9) and Young inequality it is also

(6.16)
$$\begin{aligned} J(w_\ell)-J(w) &\le (\sigma_\ell-\sigma,\varepsilon(u_\ell-u))_{L^2(\Omega;\mathbb{R}^{d\times d})}\\ &\le \frac{1}{K}\|\sigma_\ell-\sigma\|^2_{L^2(\Omega;\mathbb{R}^{d\times d}_{sym})} + \frac{K}{4}\|w-w_\ell\|^2_{\mathcal{H}}\,.\end{aligned}$$

Using (6.15) to bound (6.16) from above, one arrives at

(6.17)
$$\begin{aligned} J(w_\ell)-J(w) &\le \frac{1}{K}\|\sigma_\ell-\sigma\|^2_{L^2(\Omega;\mathbb{R}^{d\times d}_{sym})} + \frac{K}{4}\|w-w_\ell\|^2_{\mathcal{H}}\\ &\le \frac{1}{K}\|\sigma_\ell-\sigma\|^2_{L^2(\Omega;\mathbb{R}^{d\times d}_{sym})} + \frac{1}{2}(J(w_\ell)-J(w))\,,\end{aligned}$$

that is,

$$J(w_\ell)-J(w) \le \frac{2}{K}\|\sigma_\ell-\sigma\|^2_{L^2(\Omega;\mathbb{R}^{d\times d}_{sym})} \le \frac{2}{K\Lambda}\||\sigma_\ell-\sigma|\|^2_{\mathbb{C}^{-1};\Omega}\,, \tag{6.18}$$

where we have accounted for (2.2) and (2.3). The reliability estimate (4.16) in (6.18) yields

$$J(w_\ell)-J(w) \le \frac{4}{K\Lambda}C_{rel}^2(\eta_\ell^2+\mathrm{osc}_\ell^2(f))\,, \tag{6.19}$$

and together with the bulk criterion (5.1) one obtains

$$J(w_\ell)-J(w) \le \frac{4}{K\Lambda}C_{rel}^2(\frac{1}{\Theta}\sum_{E\in\mathcal{M}_\ell}\eta_E^2+\mathrm{osc}_\ell^2(f))\,. \tag{6.20}$$

Using the discrete efficiency estimates (6.2) and (6.3), and the finite overlap between patches one arrives at

$$J(w_\ell)-J(w) \le \alpha_1\||\sigma_\ell-\sigma_{\ell+1}|\|^2_{\mathbb{C}^{-1};\Omega} + \alpha_2(\mathrm{osc}_\ell^2(f)+\mathrm{osc}_\ell^2(g))\,, \tag{6.21}$$

with

$$\alpha_1 = 8C_{rel}^2C_M^2D/(\Theta K\Lambda)$$

and

$$\alpha_2 = \max\{8C_{rel}^2C_2^2D/(\Theta K\Lambda),\, 4C_{rel}/(K\Lambda)(2C_1^2D/\Theta+1)\}\,,$$

where $D \in \mathbb{N}$ accounts for the overlapping of the patches. Given the inequality

$$\|\|\sigma_\ell - \sigma_{\ell+1}\|\|^2_{\mathbb{C}^{-1};\Omega} \leq 2(J(w_\ell) - J(w_{\ell+1})) \tag{6.22}$$

as a result of (4.3) with $\mathcal{H}_{\ell+1}$ in place of $\mathcal{H}$, setting $\delta_\ell := J(w_\ell) - J(w)$, and $\delta_{\ell+1} := J(w_{\ell+1}) - J(w)$, from (6.21) one then obtains

$$\delta_{\ell+1} \leq (1 - \frac{1}{2\alpha_1})\delta_\ell + \frac{\alpha_2}{\alpha_1}(\mathrm{osc}^2_\ell(f) + \mathrm{osc}^2_\ell(g))\,, \tag{6.23}$$

which is (6.1) with $\rho_E := 1 - 1/\alpha_1$ and $\rho = \alpha_2/\alpha_1$. □

Remark 6.1. *As for the possible values of ρ_E, from the definition of α_1, it results $0 < \rho_E \leq 1$ with $\rho_E \to 1$ for $C_{rel} \to \infty$, or $C_M \to \infty$, or $K \to 0$. These conditions are associated with $\nu \to 1/2$ and hardening moduli approaching to zero. The latter condition corresponds to perfect plasticity that will be analysed in Section 6.4.*

6.2. **Data oscillation reduction.** Equation (6.1) shows the convergence of the energies provided that one can ensure for instance the data oscillation reduction, i.e. the existence of positive constants $\rho_f < 1$ and $\rho_g < 1$ depending on the regularity of the initial triangulation $\mathcal{T}_0$ such that

$$\mathrm{osc}^2_{\ell+1}(f) \leq \rho_f \mathrm{osc}^2_\ell(f)\,, \tag{6.24}$$

and

$$osc^2_{\ell+1}(g) \leq \rho_g osc^2_\ell(g)\,. \tag{6.25}$$

The conditions (6.24) and (6.25) follow, for instance, from the selection strategies (5.2) and (5.3) along with red-refinement of the elements belonging to $\Omega_{j,\ell}$ for $j \in \hat{\mathcal{K}}_\ell$ and of those having an edge in $\hat{\mathcal{E}}_\ell(\Gamma_N)$, respectively. Recall from Section 5.1 that $\hat{\mathcal{K}}_\ell$ and $\hat{\mathcal{E}}_\ell(\Gamma_N)$ denote the set of selected free node- and Neumann edge-patches according to (5.2) and (5.3), respectively.

Proof of (6.24). The proof is given for steps.

1*st step:* Given $j \in \hat{\mathcal{K}}_\ell$ and the node patch $\Omega_{j,\ell}$ of $\mathcal{T}_\ell$, we first relate the oscillations on the refined patches $\mathrm{osc}^2_{\ell+1}(f;\Omega_{j,\ell})$ to the coarse one $\mathrm{osc}^2_{j,\ell}(f;\Omega_{j,\ell})$. Without loss of generality, and to illustrate our arguments, we set $j = 0 \in \hat{\mathcal{K}}_\ell$ and consider the patch $\Omega_{0,\ell}$ with all the elements red-refined shown in Figure 7.
By a careful consideration of the overlapping between the patches in $\mathcal{T}_{\ell+1}$ and with the notation of Figure 7 we can write

$$\begin{aligned}\|f - f_{0,\ell}\|^2_{L^2(\Omega_{0,\ell})} = &\sum_{i=0}^{6} \|f - f_{0,\ell}\|^2_{L^2(\Omega_{i,\ell+1})} - \sum_{i=1}^{7} \|f - f_{0,\ell}\|^2_{L^2(T_{i,\ell+1})} \\ &- 2\|f - f_{0,\ell}\|^2_{L^2(\Omega_{0,\ell+1})} - \|f - f_{0,\ell}\|^2_{L^2(T_{4,\ell+1})}\,.\end{aligned} \tag{6.26}$$

Noting that

$$\begin{aligned}&\|f - f_{0,\ell}\|^2_{L^2(\Omega_{0,\ell+1})} + \sum_{i=1}^{7} \|f - f_{0,\ell}\|^2_{L^2(T_{i,\ell+1})} \leq \|f - f_{0,\ell}\|^2_{L^2(\Omega_{0,\ell})}\,, \\ &\|f - f_{0,\ell}\|^2_{L^2(\Omega_{0,\ell+1})} + \|f - f_{0,\ell}\|^2_{L^2(T_{4,\ell+1})} \leq \|f - f_{0,\ell}\|^2_{L^2(\Omega_{0,\ell})}\,,\end{aligned} \tag{6.27}$$

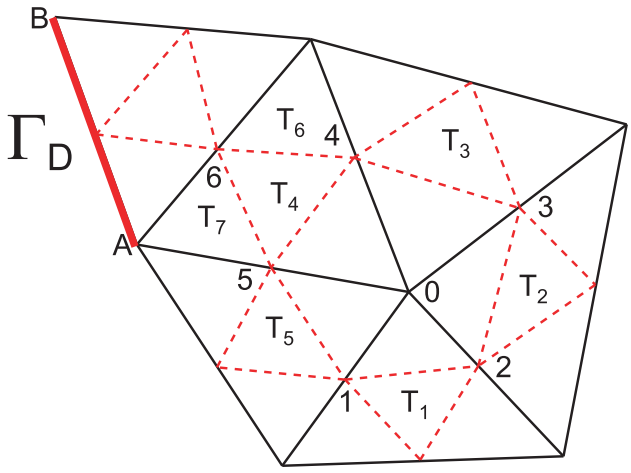

FIGURE 7. The node patch $\Omega_{0,\ell}$ is red-refined with creation of new nodes of $\mathcal{K}_{\ell+1}$. The segment AB is part of Γ_D and the fix node A has been assigned to the free node 0.

after combining (6.27) and (6.26) and some rearrangements we obtain

$$\sum_{i=0}^{6} \|f - f_{0,\ell}\|^2_{L^2(\Omega_{i,\ell+1})} \leq 3\|f - f_{0,\ell}\|^2_{L^2(\Omega_{0,\ell})}\,. \tag{6.28}$$

Since $f_{i,\ell+1}$ is the L^2 projection of f onto the space of constant functions defined over $\Omega_{i,\ell+1}$ we have also

$$\sum_{i=0}^{6} \|f - f_{i,\ell+1}\|^2_{L^2(\Omega_{i,\ell+1})} \leq \sum_{i=0}^{6} \|f - f_{0,\ell}\|^2_{L^2(\Omega_{i,\ell+1})}$$

that together with (6.28) yields

$$\sum_{i=0}^{6} \|f - f_{i,\ell+1}\|^2_{L^2(\Omega_{i,\ell+1})} \leq 3\|f - f_{0,\ell}\|^2_{L^2(\Omega_{0,\ell})}\,. \tag{6.29}$$

If we set $h_{i,\ell+1} = \alpha_0 h_{0,\ell}$ for $0 \leq i \leq 6$ and $\alpha_0 \in]0,1[$ to be chosen later, then we have

$$\sum_{i=0}^{6} h^2_{i,\ell+1}\|f - f_{i,\ell+1}\|^2_{L^2(\Omega_{i,\ell+1})} \leq 3\alpha_0^2\, h^2_{0,\ell}\, \|f - f_{0,\ell}\|^2_{L^2(\Omega_{0,\ell})} \tag{6.30}$$

that is, for $j \in \hat{\mathcal{K}}_\ell$ we obtain the following bound

$$\mathrm{osc}^2_{\ell+1}(f;\Omega_{j,\ell}) \leq 3\alpha_0^2\, \mathrm{osc}^2_{j,\ell}(f;\Omega_{j,\ell})\,. \tag{6.31}$$

2nd Step: We now relate the oscillations $\mathrm{osc}^2_{\ell+1}(f;\Omega_{j,\ell})$ to $\mathrm{osc}^2_{\ell}(f;\Omega_{j,\ell})$ for the node patches not selected for the control of the volume oscillation. Following arguments similar to the previous step, it is not difficult to realize that for $j \in \mathcal{K} \setminus \hat{\mathcal{K}}_\ell$ there holds

$$\mathrm{osc}^2_{\ell+1}(f;\Omega_{j,\ell}) \leq \mathrm{osc}^2_{j,\ell}(f;\Omega_{j,\ell})\,. \tag{6.32}$$

3rd Step: Since only the node patches with $j \in \hat{\mathcal{K}}_\ell$ are refined for oscillation control, using (6.31) and (6.32) we can write

$$\begin{aligned}\operatorname{osc}^2_{\ell+1}(f;\Omega) &= \sum_{j\in\mathcal{K}_\ell} \operatorname{osc}^2_{\ell+1}(f;\Omega_{j,\ell}) \\ &= \sum_{j\in\hat{\mathcal{K}}_\ell} \operatorname{osc}^2_{\ell+1}(f;\Omega_{j,\ell}) + \sum_{j\in\mathcal{K}_\ell\setminus\hat{\mathcal{K}}_\ell} \operatorname{osc}^2_{\ell+1}(f;\Omega_{j,\ell}) \\ &\leq 3\alpha_0^2 \sum_{j\in\hat{\mathcal{K}}_\ell} \operatorname{osc}^2_{j,\ell}(f;\Omega_{j,\ell}) + \sum_{j\in\mathcal{K}_\ell\setminus\hat{\mathcal{K}}_\ell} \operatorname{osc}^2_{j,\ell}(f;\Omega_{j,\ell})\,.\end{aligned} \tag{6.33}$$

Adding and subtracting $\sum_{j\in\hat{\mathcal{K}}_\ell} \operatorname{osc}^2_{j,\ell}(f;\Omega_{j,\ell})$ on the right hand side of (6.33), the bulk criterion (5.2) for volume oscillation control, and $\alpha_0 \in]0, \sqrt{3}/3[$ so that $3\alpha_0^2 - 1 < 0$ yield

$$\begin{aligned}\operatorname{osc}^2_{\ell+1}(f;\Omega) &\leq \operatorname{osc}^2_{\ell}(f;\Omega) + (3\alpha_0^2 - 1) \sum_{j\in\hat{\mathcal{K}}_\ell} \operatorname{osc}^2_{j,\ell}(f;\Omega_{j,\ell}) \\ &\leq (1 - (1 - 3\alpha_0^2)\Theta_f)\operatorname{osc}^2_{\ell}(f;\Omega)\,.\end{aligned} \tag{6.34}$$

Let $\rho_f := (1 - (1 - 3\alpha_0^2)\Theta_f)$, we complete the proof by choosing $\alpha_0 \in]0, \sqrt{3}/3[$ and $\Theta_f \in]0, 1[$ so that $\rho_f < 1$. This is, for instance the case, with $\alpha_0 = 1/2$ and $\Theta_f = 1/2$. □

Proof of (6.25). Apply similar arguments as for (6.24). □

6.3. **Convergence of stresses.** We recall that a sequence $(y_n)_{n\in\mathbb{N}}$ of real nonnegative numbers convergent to zero is said to be $R-$linear convergent if it is bounded from above by a $Q-$linear infinitesimal convergent sequence $(z_n)_{n\in\mathbb{N}}$ [31], that is,

$$y_n \leq z_n$$

where for $r \in]0, 1[$ it is

$$z_{n+1} \leq r z_n \text{ for all } n \text{ sufficiently large}\,.$$

From (4.3) and (6.1), after some rearrangements, by induction we obtain

$$|||\sigma - \sigma_\ell|||_{\mathbb{C}^{-1};\Omega} \leq 2(\sqrt{\rho_E})^\ell \sqrt{\delta_0} + 2C(\ell - 1)\rho^{\ell-1} \operatorname{osc}_0, \tag{6.35}$$

with $0 < \rho = \max\{\sqrt{\rho_E}, \sqrt{\rho_f}, \sqrt{\rho_g}\} < 1$ and $\operatorname{osc}_0^2 = \operatorname{osc}_0^2(f) + \operatorname{osc}_0^2(g)$. Equation (6.35) shows the error on the stresses being bounded from above by the sum of two linear convergent sequences, proving so the $R-$linear convergence of the stresses with respect to the numeber ℓ of refinements.

6.4. **Perfect Plasticity.** As pointed out in Remark 6.1, for vanishing hardening moduli $\rho_E \to 1$. As a result, one cannot conclude neither the energy reduction nor the $R-$linear convergence of the stresses. Furthermore, neither the primal formulation nor the displacement formulation are well posed using the Sobolev space V for the deformation u, but one must use the space of the bounded deformations,

i.e. the space of the vector functions that are integrable and with the corresponding strains being bounded measures [35]. Using a standard result of convex analysis for W convex, $C^1(\mathbb{R}^{d\times d}_{sym})$, and with Lipschitz derivative, the energy density W for perfect plasticity meets the following inequalities (see [22, Exercise 2.7] and [9] for a direct proof of the inequality)

$$\frac{1}{2}|\sigma_1-\sigma_2|^2_{\mathbb{C}^{-1}} \le (\sigma_1-\sigma_2)\colon(\varepsilon_1-\varepsilon_2) \tag{6.36}$$

$$\frac{1}{2}|\sigma_1-\sigma_2|^2_{\mathbb{C}^{-1}} \le W(\varepsilon_1)-W(\varepsilon_2)-\sigma_2:(\varepsilon_1-\varepsilon_2)\,, \tag{6.37}$$

with $\sigma_i := DW/D\varepsilon|_{\varepsilon=\varepsilon_i}$ $i=1,2$.
Strong convergence of stresses obtained by the displacement formulation can be however established under the assumption that $u \in V$. Under this condition, then we can state

$$u=\arg\min_{v\in V}\int_\Omega W(\varepsilon(v))\,dx-b(v) \text{ and } u_\ell=\arg\min_{v_\ell\in V_\ell}\int_\Omega W(\varepsilon(v_\ell)\,dx-b(v_\ell)\,, \tag{6.38}$$

and it is also

$$(\sigma-\sigma_\ell,\varepsilon(v_\ell))_{L^2(\Omega;\mathbb{R}^{d\times d})}=0 \quad \text{for all } v_\ell\in V_\ell\,. \tag{6.39}$$

Integration over Ω of both sides of (6.36) with $\varepsilon_1=\varepsilon(u)$ and $\varepsilon_2=\varepsilon(u_\ell)$, and (6.39) yield

$$|||\sigma-\sigma_\ell|||^2_{\mathbb{C}^{-1};\Omega} \le \int_\Omega(\sigma-\sigma_\ell)\colon(\varepsilon(u-\mathcal{J}(u)))\,, \tag{6.40}$$

with the quasinterpolation operator $\mathcal{J}$ defined in Section 4.2. Following similar arguments as in Section 4.4 we then obtain the following estimate

$$|||\sigma-\sigma_\ell|||^2_{\mathbb{C}^{-1};\Omega} \le C(\eta_\ell+\mathrm{osc}_\ell(f))\,, \tag{6.41}$$

where we employ the boundeness of $\|Du\|_{L^2(\Omega;\mathbb{R}^{d\times d})}$.

Remark 6.2. *Notice the loss of the exponent in the reliability estimate* (6.41) *compared to* (4.16).

The bulk criterion (5.1) and the local discrete efficiency estimates (6.2) and (6.3), together with the bound

$$|||\sigma_{\ell+1}-\sigma_\ell|||^2_{\mathbb{C}^{-1};\Omega} \le J(u_\ell)-J(u_{\ell+1})\,, \tag{6.42}$$

yield in (6.41) the following

$$|||\sigma-\sigma_\ell|||^2_{\mathbb{C}^{-1};\Omega} \le C((J(u_\ell)-J(u_{\ell+1}))^{1/2}+\mathrm{osc}_\ell(f)+\mathrm{osc}_\ell(g)) \tag{6.43}$$

The bound (6.42) is obtained using twice (6.37) with ε_1 and ε_2 as $\varepsilon(u_\ell)$ and $=\varepsilon(u_{\ell+1})$ and integrating over Ω.
Since $\delta_\ell := J(u_\ell)-J(u)$ is a monotone decreasing sequence of non negative real numbers, it is a Cauchy sequence, that is

$$\lim_{\ell\to\infty}(\delta_\ell-\delta_{\ell+1})=0\,,$$

that together with (6.43) delivers the convergence of the stresses provided that $\mathrm{osc}_\ell\to 0$ as $\ell\to\infty$.

7. Numerical examples

For vanishing data oscillations such as in the case of $f = const$ and $g = const$ considered in the numerical examples of this section, the Algorithm 5.1 can be simplified as follows

Algorithm 7.1.
Input a coarse shape-regular triangulation $\mathcal{T}_0$ of Ω into triangles with set of edges $\mathcal{E}_0$, $0 < \Theta < 1$, and repeat $(a) - (f)$.

(a) `SOLVE`*: Solve the nonlinear discrete problem,*

$$w_\ell = \underset{z_\ell \in \mathcal{H}_\ell}{arg\ min}\ J(z_\ell) \text{ and set } \sigma_\ell := \mathbb{C}(\varepsilon(u_\ell) - p_\ell)\,.$$

(b) `ESTIMATE`*: Given any $E \in \mathcal{E}_\ell$ with measure h_E, compute*

$$\eta_E^2 := h_E \int_E |J_E|^2\, ds \text{ for each } E \in \mathcal{E}_\ell \text{ and } \eta_\ell = (\sum_{E\in\mathcal{E}_\ell} \eta_E^2)^{1/2}\,.$$

(c) `MARK`*: Select a subset $\mathcal{M}_\ell$ of $\mathcal{E}_\ell$ in the current triangulation $\mathcal{T}_\ell$ with*

$$\Theta\eta_\ell^2 \le \sum_{E\in\mathcal{M}_\ell} \eta_E^2\,.$$

(d) `REFINE`*: Red-refine all the elements T with some edge in $\mathcal{M}_\ell$.*

(e) *Run the closure algorithm with red-green-blue refinement* [40]*. Denote with $\mathcal{T}_{\ell+1}$ the resulting shape-regular triangulation with associated discrete space $\mathcal{H}_{\ell+1}$.*

(f) *Set $\ell := \ell + 1$ and go to* ***(a)****.*

Output discrete stress fields σ_0, σ_1, ...σ_ℓ, ... in $L^2(\Omega;\mathbb{R}^{d\times d}_{sym})$ as approximation to $\sigma = \mathbb{C}(\varepsilon(u) - p)$.

The main and substantial difference consists in removing the inner node property, i.e. the use of `bisec5(T)` for the elements marked for error reduction. An adaption of the proof of (6.2) and (6.3) using the edge based discrete function ϕ_{m_E} shows the following local discrete efficiency estimate

$$\|h_E^{1/2} J_E\|_{L^2(E;\mathbb{R}^d)} \le C_M |||\sigma_\ell - \sigma_{\ell+1}|||_{\mathbb{C}^{-1};\omega_E}$$

with ω_E from (6.5). Following the arguments used for proving (6.1) and (6.35), one can easily obtain the energy reduction and $R-$linear convergence of the stresses for the Algorithm 7.1.

Remark 7.1. *In the implementation of the step* `MARK`*, we first sort the edges in decreasing order according to the value of their contribution η_E to the estimate η_ℓ and then pick the first one that realize the condition (c).*

The reliability constant that enters the estimate (6.41) depends on the regularity of the initial mesh, and the material properties. Since the adopted refinement rules preserve this regularity also for the refined meshes [7], and the material constants are constant during the refinement process, in the examples of this section we compare

the convergence rate of η from (4.14) with respect to the number of degrees of freedom and of refinement loops for uniform and adaptive refinements according to Algorithm 7.1 and Algorithm 7.2 given below. The latter uses the max refinement rule (1.2) as step `MARK` and is defined as follows.

Algorithm 7.2.
Input a coarse shape-regular triangulation $\mathcal{T}_0$ of Ω into triangles with set of edges $\mathcal{E}_0$, $0 < \Theta < 1$, and repeat $(a) - (f)$.

(a) `SOLVE`*: Solve the nonlinear discrete problem,*

$$w_\ell = \underset{z_\ell \in \mathcal{H}_\ell}{arg\ min}\ J(z_\ell) \text{ and set } \sigma_\ell := \mathbb{C}(\varepsilon(u_\ell) - p_\ell)\,.$$

(b) `ESTIMATE`*: Given any $E \in \mathcal{E}_\ell$ with measure h_E, compute*

$$\eta_E^2 := h_E \int_E |J_E|^2\, ds \text{ for each } E \in \mathcal{E}_\ell\,.$$

(c) `MARK`*: Select a subset $\mathcal{M}_\ell$ of $\mathcal{E}_\ell$ in the current triangulation $\mathcal{T}_\ell$ with*

$$\Theta \max_{F \in \mathcal{E}_\ell} \eta_F \le \eta_E \quad \text{for all } E \in \mathcal{M}_\ell\,. \tag{7.1}$$

(d) `REFINE`*: Red-refine all the elements T with some edge in $\mathcal{M}_\ell$.*

(e) *Run the closure algorithm with red-green-blue refinement* [40]*. Denote with $\mathcal{T}_{\ell+1}$ the resulting shape-regular triangulation with associated discrete space $\mathcal{H}_{\ell+1}$.*

(f) *Set $\ell := \ell + 1$ and go to* ***(a)****.*

Output discrete stress fields σ_0, σ_1, ...σ_ℓ, ... in $L^2(\Omega; \mathbb{R}^{d\times d}_{sym})$ as approximation to $\sigma = \mathbb{C}(\varepsilon(u) - p)$.

Remark 7.2. *We recall that the issue of convergence for the Algorithm 7.2 remains still unsolved for higher dimensions for elliptic problems* [1].

In the first two examples of this section we consider the model of multiyield plasticity described in Section 3.3. For the algorithmic details of the solution of the incremental constitutive value problem by an alternating direction algorithm we refer to [3]. The last example describes the AFEM for a benchmark problem with perfect plasticity.

7.1. **L-shape domain.**

We consider the L-shape domain $\Omega = (0,1)^2 \setminus (0,0.5)^2$ with vanishing volume force f, boundary conditions, and material properties depicted in Figure 8 together with the coarse mesh $\mathcal{T}_0$.

For this problem the exact solution is not known. For linear elastic behaviour singularities of the solution are localized at the reentrant corner and at the discontinuity of the type of boundary conditions, that is, at the points $(1,0)$ and $(2,0)$. We therefore expect a similar behaviour also in the case of incremental plasticity, with first plastic loading in the neighborhood of the singular points, and then spreading over the other parts of the domain that have remained elastic. Given the non uniform distribution of the strain, we want to investigate the adaptive finite element algorithms described in this section as tool to capture the singular zones and by product

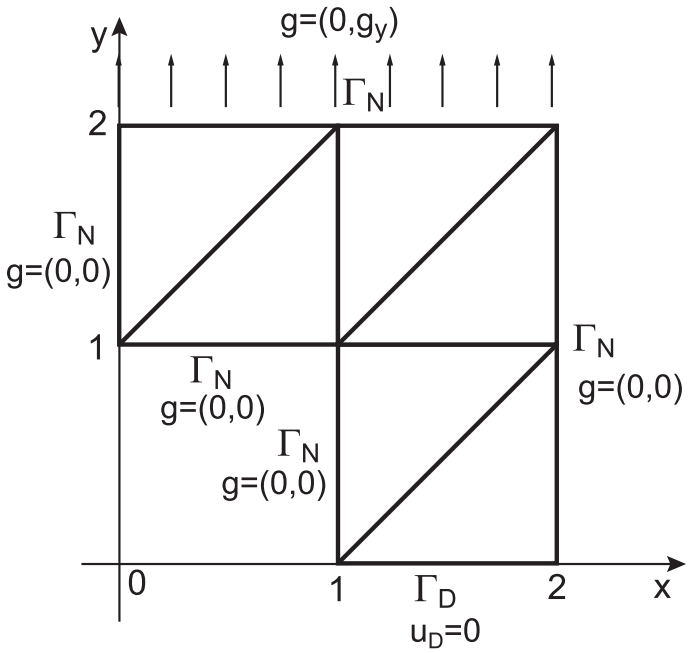

$g_y = 5$

$\lambda = 1000, \quad \mu = 1000$

$\sigma_{1,y} = 5, \quad h_1 = 100$

$\sigma_{2,y} = 7, \quad h_2 = 50$

FIGURE 8. Example 7.1: Geometry for the L-shape domain with Dirichlet boundary conditions $u_D = 0$ on Γ_D and applied load $g_y = 5$ on the boundary Γ_N at $y = 2$. The reentrant corner, and the discontinuity points $(1, 0)$ and $(2, 0)$ represent singularity points.

to improve the convergence compared to uniform refinements. With this regard, Figure 9 compares the convergence rates of η for uniform and adaptive refinements based on (1.3) and (1.2). We notice that the uniform mesh-refinement converges only sub-optimally due to the poor regularity of the solution, as expected, while the adaptive mesh-refinements realised both by the Algorithm 7.1 and Algorithm 7.2 recover optimal convergence rates, also on occurrence of plastic deformations. Figure 10, on the other hand, compares the performance of the two algorithms in terms of the number of refinement loops necessary to reduce the error of a fixed fraction. Here we notice the better performance of the adaptive algorithm based on the bulk criterion. Furthermore, the Algorithm 7.1 shows a $Q-$linear convergence rate, despite our theoretical findings of $R-$linear convergence rate. Finally, Figure 11 depicts the triangulations generated with the Algorithm 7.1 superimposed to the plot of the plastic zones showing a local higher refinements towards the reentrant corner where also the second yield surface is activated and at the discontinuity points of the type of boundary conditions. Figure

7.2. **Cook's membrane problem.**
The problem consists of a trapezoidal plate clamped on one end and loaded by a uniformly distributed in-plane bending load on the other end, as shown in Figure 12. We consider the same material model as in the previous example, with material

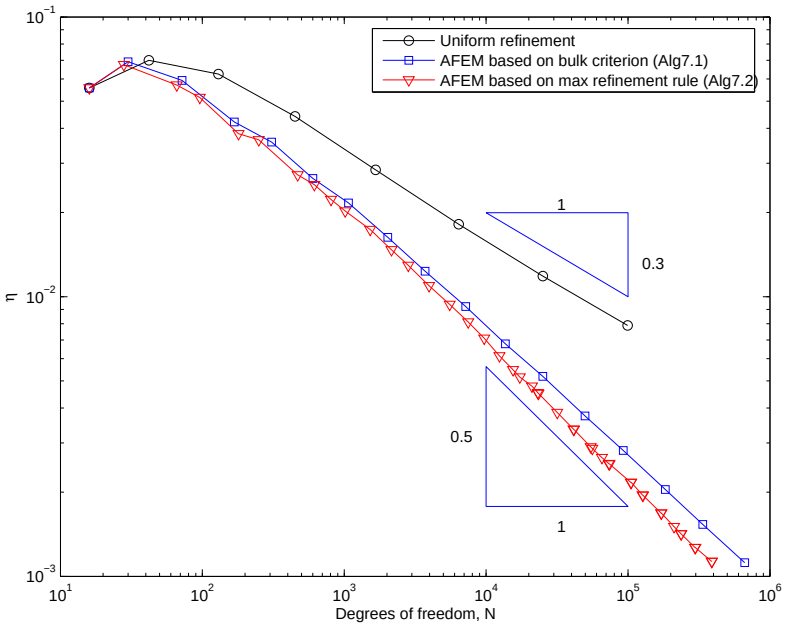

FIGURE 9. Example 7.1: Convergence history of η_ℓ for uniform and adaptive finite element refinements based on the bulk criterion (1.3) computed by Algorithm 7.1 with $\Theta = 0.5$, and on the max refinement rule (1.2) computed by Algorithm 7.2 with $\Theta = 0.5$. Each adaptive algorithm performs with a convergence rate with respect to the number of degree of freedom of about 0.5 in contrast to 0.3 for uniform refinement. This corresponds to the empirical convergence rate of 1 and 0.6, respectively, with respect to a (uniform) mesh size h.

parameters reported also in Figure 12. The applied load is such that the two yield surfaces are activated.
Likewise the previous example, we test the performance of the adaptive finite element Algorithms 7.1 and 7.2. Both the algorithms lead to a slightly better order of experimental convergence displayed in Figure 13 compared to uniform refinement. Figure 14, on the other hand, compares the convergence rate with respect to the number of refinement loops displaying a linear convergence rate for Algorithm 7.1 as opposite to the one displayed by the AFEM based on the max refinement rule. The triangulations generated by the Algorithm 7.1 based on η, reported in Figure 15, show local mesh refinement towards the upper left corner where a change of the type of boundary conditions causes a singularity, and at the right end where point loads are applied.

7.3. **Finite strip with a hole: perfect plasticity.**

In this example, we consider the benchmark problem with perfect plasticity described in [36]. The geometry and material properties are shown in Figure 16.
Since the applied load p is lower than the critical load p_{cr} in correspondence of which slip lines can occur, we can formulate our problem in the functional setting of the

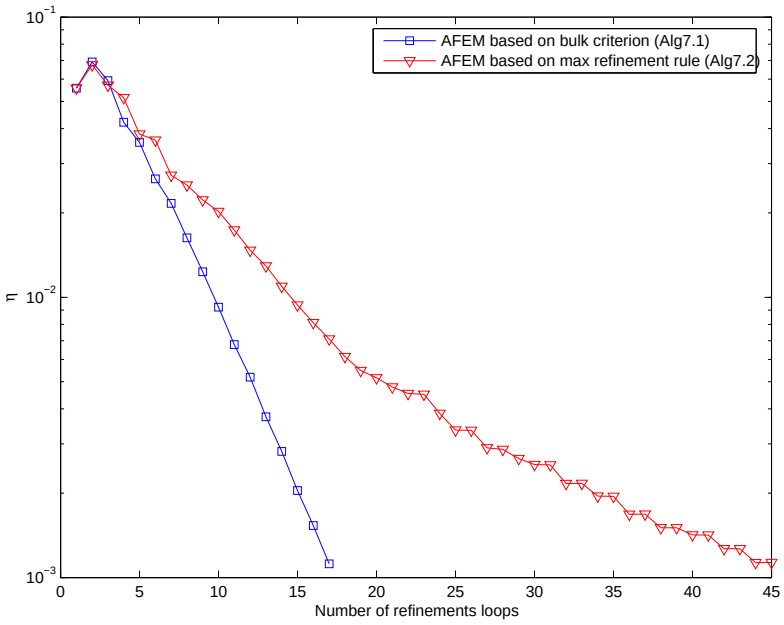

FIGURE 10. Example 7.1: Convergence history of η_ℓ with respect to the number of refinement loops for the adaptive finite element refinements based on the bulk criterion (1.3) computed by Algorithm 7.1 with $\Theta = 0.5$, and on the max refinement rule (1.2) computed by Algorithm 7.2 with $\Theta = 0.5$. The AFEM based on (1.3) performs with a linear convergence rate which is better than the one displayed by the AFEM based on (1.2).

Sobolev spaces. Convergence rate of η_ℓ for uniform and the adaptive finite element refinements based on the bulk criterion (1.3) and on the max refinement rule (1.2) are displayed in Figure 17. Both the adaptive algorithms improve the convergence rate in contrast to uniform refinement. Figure 18 compares the convergence rate for the two Algorithms 7.1 and 7.2 with respect to the number of refinement loops, showing the better performance of the Algorithm 7.1 based on the bulk criterion. Though not implied by our theoretical findings, the Algorithm 7.1 displays a linear convergence also in the case of perfect plasticity.

8. Concluding remarks

In this paper we have established an adaptive finite element algorithm (Algorithm 5.1) based on the bulk criterion introduced by [17] for the solution of a variational inequality of second kind. The latter serves as model of one time step of the primal probem of elastoplasticity with positive hardening and perfect plasticity. Our main theoretical findings can be summarized as follows:

(i) *node-patch oscillation reduction*: With the oscillations defined by (4.11) and (4.13), there exist positive constants $\rho_f < 1$ and $\rho_g < 1$, depending on the regularity

of the initial triangulation $\mathcal{T}_0$, such that

$$\mathrm{osc}^2_{\ell+1}(f) \le \rho_f \mathrm{osc}^2_\ell(f) \quad \text{and} \quad \mathrm{osc}^2_{\ell+1}(g) \le \rho_g \mathrm{osc}^2_\ell(g)\,.$$

(*ii*) *energy reduction*: There exist positive constants ρ_E, C with $\rho_E < 1$, and $\rho = \max\{\rho_E, \rho_f, \rho_g\} < 1$, depending on the regularity of the initial triangulation $\mathcal{T}_0$ and on the material parameters, such that

$$\delta_\ell \le \rho_E^\ell \delta_0 + C(\ell-1)\rho^{\ell-1}\mathrm{osc}_0^2\,,$$

where we have set $\mathrm{osc}_0^2 = \mathrm{osc}_0^2(f) + \mathrm{osc}_0^2(g)$.
(*iii*) *R−linear convergence of the stresses*: With the previous notations, there holds

$$|||\sigma - \sigma_\ell|||_{\mathbb{C}^{-1};\Omega} \le 2(\sqrt{\rho_E})^\ell \sqrt{\delta_0} + 2C(\ell-1)\rho^{\ell-1}\,\mathrm{osc}_0\,.$$

For perfect plasticity, we prove only the convergence of the stresses, though our numerical results display a linear convergence rate also in this case.

In comparing numerically the performance of the AFEM with the step `MARK` based on (1.2) and on (1.3), we verify for both the algorithms an improved convergence rate with respect to the number of degree of freedom compared to the uniform refinement. In evaluating the convergence with respect to the number of refinement loops, on the other hand, we observe that the AFEM based on (1.3) displays a better convergence rate than the one displayed using the max refinement rule, currently used in the engineering literature.
In conclusion, the theoretical analysis given in this paper together with our numerical experiments suggest the better performance of the AFEM with the step `MARK` based on (1.3) compared to the one using (1.2), frequently adopted in practice. The implementation of (1.3) also does not incure additional efforts compared to the use of (1.2).

Acknowledgements

The author AO would like to thank the support by the DFG through the priority program 1095 "Analysis, Modeling and Simulation of Multiscale Problems" whereas JV acknowledges the Austrian Science Fund 'Fonds zur Förderung der wissenschaftlichen Forschung (FWF)' for the support under grant SFB F013/F1306 in Linz, Austria.

References

[1] Babuska I., Vogelius M., Feedback and adaptive finite elment solution of one-dimensional boundary value problems, Numer. Math., 44 (1984) 75-102.
[2] Brenner S.C., Scott L.R., *The Mathematical Theory of Finite Element Methods*. Springer Verlag, New York, 2*nd* Edition, 2002
[3] Brokate M., Carstensen C., Valdman J., A quasistatic boundary value problem in multisurface elastoplasticity: Part 1 - Analysis, Math. Meth. Appl. Sciences, 2004 (27) 1697–1710.
[4] Brokate M., Carstensen C., Valdman J., A quasistatic boundary value problem in multisurface elastoplasticity: Part 2 - Numerical solution, Math. Meth. Appl. Sciences, 2004 (28) 881–901.
[5] Carstensen C., Numerical analysis of the primal problem of elastoplasticity with hardening, Numer. Math. 82 (1999) 577–597.
[6] Carstensen C., Quasi interpolation and a posteriori error analysis in finite element method, M2AN Math. Model Num. Anal. 33 (1999) 1187–1202.

[7] Carstensen C., An adaptive mesh-refining algorithm allowing for an H^1 stable L^2 projection onto Courant finite element spaces, Constructive Approximation, 20 (2004) 549-564.
[8] Carstensen C., Convergence of adaptive finite element methods in computational mechanics. *Proceedings of the Sixth World Congress on Computational Mechanics*, September 2004.
[9] Carstensen C., On the convergence of adaptive FEM for convex minimization problems, *(in progress)*.
[10] Carstensen C., Alberty J., Averaging techniques for reliable a posteriori FE–error control in elastoplasticity with hardening, Comput. Methods Appl. Mech. Engrg. 192 (2003) 1435–1450.
[11] Carstensen C., Bartels S., Each averaging technique yields reliable a posteriori error control in FEM on unstructured grids. Part I: Low order conforming, nonconforming, and mixed FEM, Math. Comp. 71 (2002) 945-969.
[12] Carstensen C., Hoppe R.H.W., Error reduction and convergence for an adaptive mixed finite element method, Math. Comp., *(accepted for publication)*.
[13] Carstensen C., Hoppe R.H.W., Convergence analysis of an adaptive nonconforming finite element method, *(in progress)*.
[14] Carstensen C., Klose R., Orlando A., Reliable and efficient equilibrated a posteriori finite element error control in elastoplasticity and elastoviscoplasticity with hardening, Comput. Methods Appl. Mech. Engrg., *(accepted for publication)*.
[15] Carstensen C., Müller S., Local stress regularity in scalar nonconvex variational problems, SIAM J. Math. Anal. 34 (2002) 495-509.
[16] Ciarlet P.G., *The Finite Element Method for Elliptic Problems*. North–Holland, New York, 1978; reprinted as SIAM Classics in Applied Mathematics, Philadelphia, 2002
[17] Dörfler W., A convergent adaptive algorithm for Poisson's equation, SIAM J. Numer. Anal. 33 (1996) 1106-1124.
[18] Dörfler W., Nochetto R.H., Small data oscillations implies the saturation assumption, Numer. Math. 91 (2002) 1–12.
[19] Ekeland I., Temam R., *Convex Analysis and Variational Problems*, North Holland Publisher, Amsterdam, 1976; reprinted as SIAM Classics in Applied Mathematics, Philadelphia, 1999.
[20] Glowinski R. *Numerical Methods for Nonlinear Variational Problems*, Springer Verlag, New York, 1984.
[21] Han W., Reddy B.D. *Plasticity. Mathematical Theory and Numerical Analysis*, Springer Verlag, New York, 1999.
[22] Hiriart-Urruty J.-B., Lemaréchal C., *Fundamentals of Convex Analysis*, Springer Verlag, Heidelberg, 1993.
[23] Johnson C., Hansbo P., Adaptive finite element methods in computational mechanics. Comput. Methods Appl. Mech. Engrg. 101 (1992) 143–181.
[24] Koiter W.T., General theorems of elasto-plastic solids, in: Sneddon I.N., Hill R. (Eds), Progress in Solid Mechanics, North Holland Publishing Company, 1960.
[25] Maugin G. A., *The Thermomechanics of Plasticity and Fracture*, Cambridge University Press, 1992.
[26] Mitchell W.F., A comparison of adaptive refinement techniques for elliptic problems, ACM Trans. Math. Softw. 10 (1989) 745-756.
[27] Morin P., Nochetto R.H., Siebert K.G., Data oscillation and convergence of adaptive FEM, SIAM J. Numer. Anal. 38 (2000) 466-488.
[28] Morin P., Nochetto R.H., Siebert K.G., Convergence of adaptive finite element methods, SIAM Review 44 (2002) 631-658.
[29] Morin P., Nochetto R.H., Siebert K.G., Local problems on stars: a posteriori error estimators, convergence, and performance, Math. Comp. 72 (2002) 1067-1097.
[30] Mróz Z., On the description of anisotropic work-hardening, J. Mech. Phys. Solids, 15 (1967) 163-175.
[31] Nocedal J., Wright S. J., *Numerical Optimization*, Springer Verlag, New York, 1999.
[32] Reddy B.D. Martin J.B., Griffin T.B., Extremal paths and holonomic constitutive laws in elastoplasticity, Q. Appl. Math. 45 (1987) 487-502.

[33] Rivara M.C., Algorithms for refining triangular grids suitable for adaptive and multigrid techniques, Int. J. Numer. Meth. Engrg. 20 (1984) 745-756.
[34] Sawischlewski E., Steinmann P., Stein E., Modelling and computation of instability phenomena in multisurface elasto-plasticity, Comp. Mech. 18 (1996) 245-258.
[35] R. Temam R., *Mathematical Problems in Plasticity*, Gauthier–Villars, Paris, 1985.
[36] The benchmark homepage of the DFG-Paketantrag, `http://www.ibnm.uni-hannover.de/Forschung/Paketantrag/Benchmarks/benchmark.html`
[37] Valdman, J., Two-yield elastoplasticity Matlab solver, Download: `http://www.sfb013.uni-linz.ac.at/~jan/solver.zip`
[38] Veeser A., Convergent adaptive finite elements for the nonlinear Laplacian, Numer. Math. 92 (2002) 743-770.
[39] Verfürth R., A review of a posteriori error estimation techniques for elasticity problems, Comput. Methods Appl. Mech. Engrg. 176 (1999) 419–440.
[40] Verfürth R., *A Review of A Posteriori Error Estimation and Adaptive Mesh-Refinement Techniques*, Wiley–Teubner, Bath, 1996

† Institut für Mathematik, Humboldt-Universität zu Berlin, Rudower Chaussee 25, D–12489 Berlin, Germany

‡ SpezialForschungsBereich F013, Johannes Kepler Universitaet Linz, Altenbergerstrasse 69, 4040 Linz, Austria.

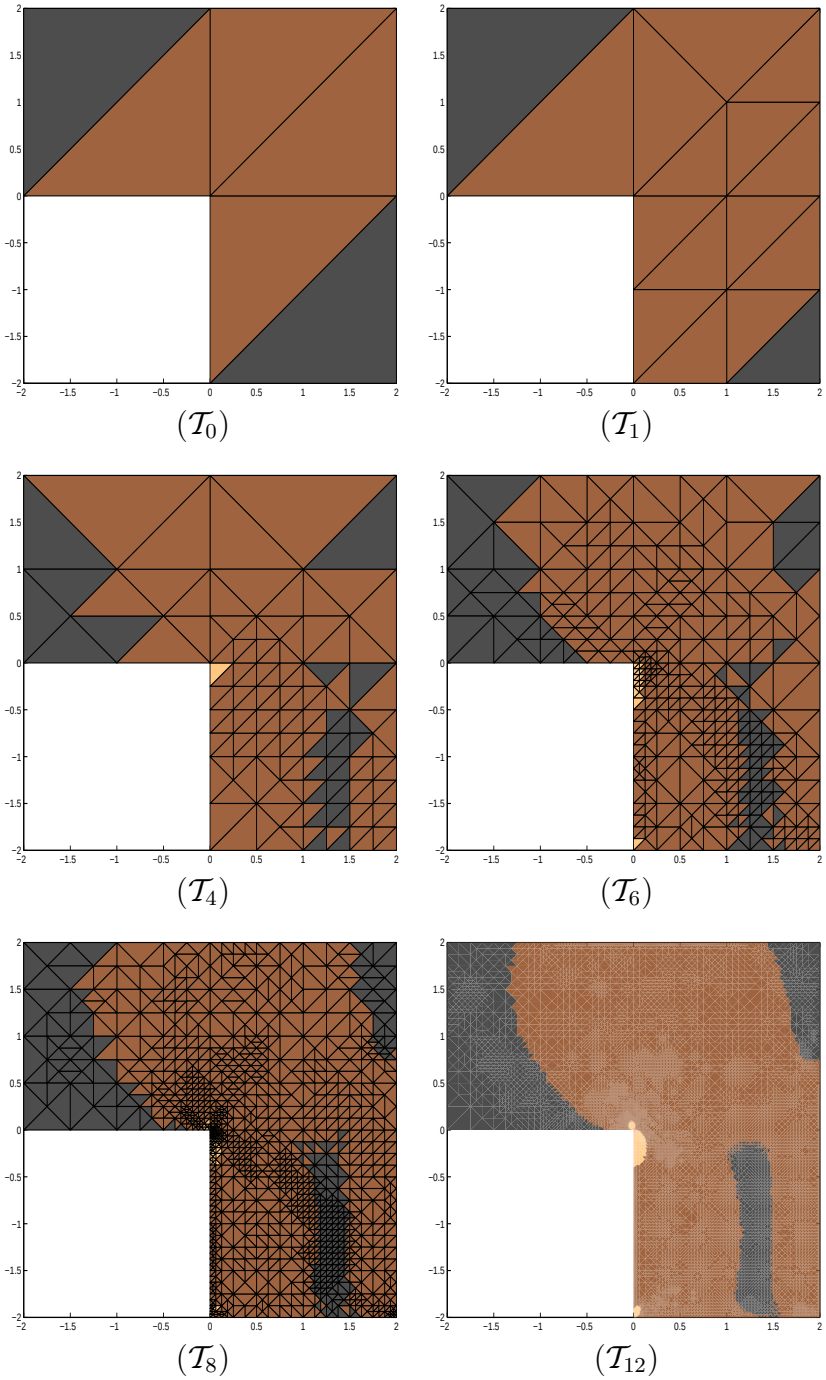

FIGURE 11. Example 7.1: Adapted triangulations $\mathcal{T}_0$, $\mathcal{T}_1$, $\mathcal{T}_4$, $\mathcal{T}_6$, $\mathcal{T}_8$, $\mathcal{T}_{12}$ for the L-shape domain generated by the Algorithm 7.1 with $\Theta = 1/2$. Notice the local higher refinement towards the reentrant corner and at the the points $(1, 0)$ and $(2, 0)$ where change of type of boundary conditions occur. The second yield surface is activated in the neighborhood of the reentrant corner and around the point $(1, 0)$. For visualization reason, $\mathcal{T}_{12}$ does not visualize the underlying mesh. Color legend: black=elastic, dark gray=first yield activated, light gray=second yield activated.

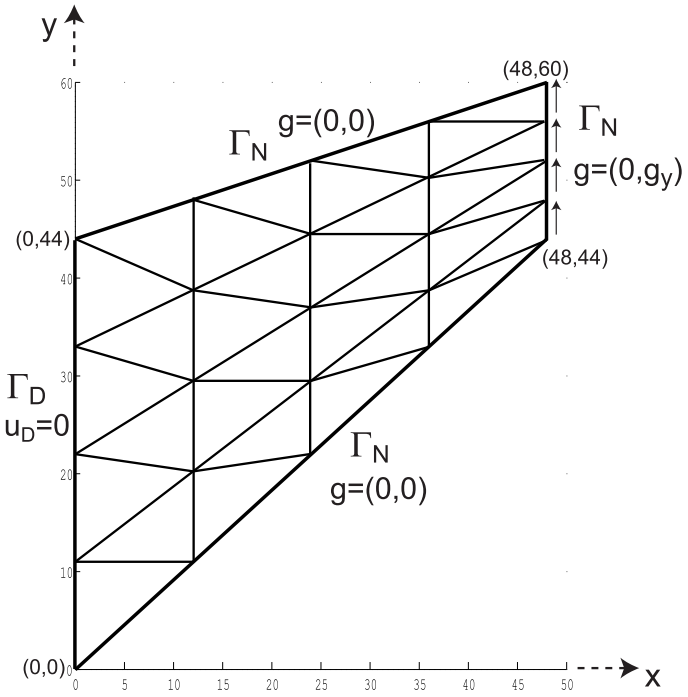

$g_y = 7.5$

$\lambda = 1000, \quad \mu = 1000$

$\sigma_{1,y} = 5, \quad h_1 = 100$

$\sigma_{2,y} = 7, \quad h_2 = 50$

FIGURE 12. Example 7.2: Geometry for the Cook membrane with $u_D = 0$ on Γ_D and applied load $g = (0, g_y)$ on the part of Γ_N with equation $x = 48$.

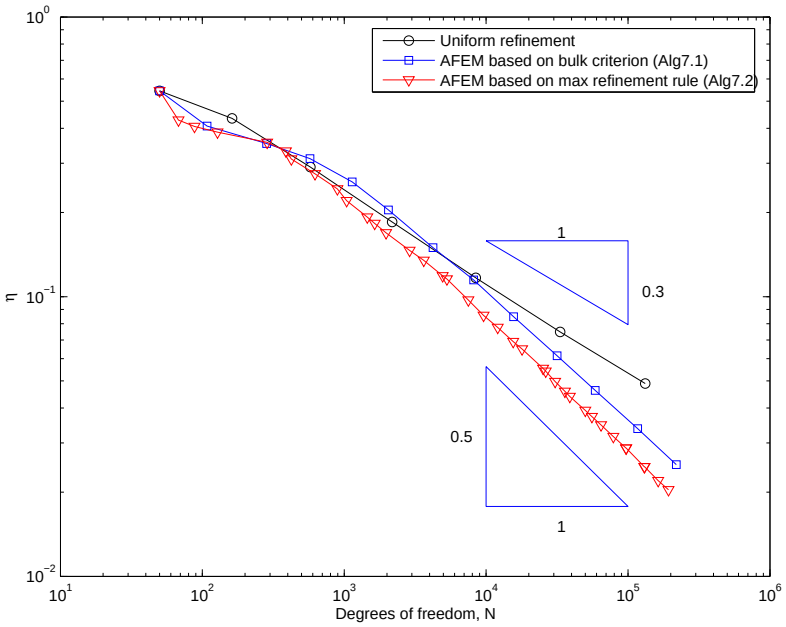

FIGURE 13. Example 7.2: Convergence history of η_ℓ for uniform and adaptive finite element refinements based on the bulk criterion (1.3) computed by Algorithm 7.1 with $\Theta = 0.5$, and on the max refinement rule (1.2) computed by Algorithm 7.2 with $\Theta = 0.5$. Each adaptive algorithm performs with a convergence rate with respect to the number of degree of freedom of about 0.5 in contrast to 0.3 for uniform refinement. This corresponds to the empirical convergence rate of 1 and 0.6, respectively, with respect to a (uniform) mesh size h.

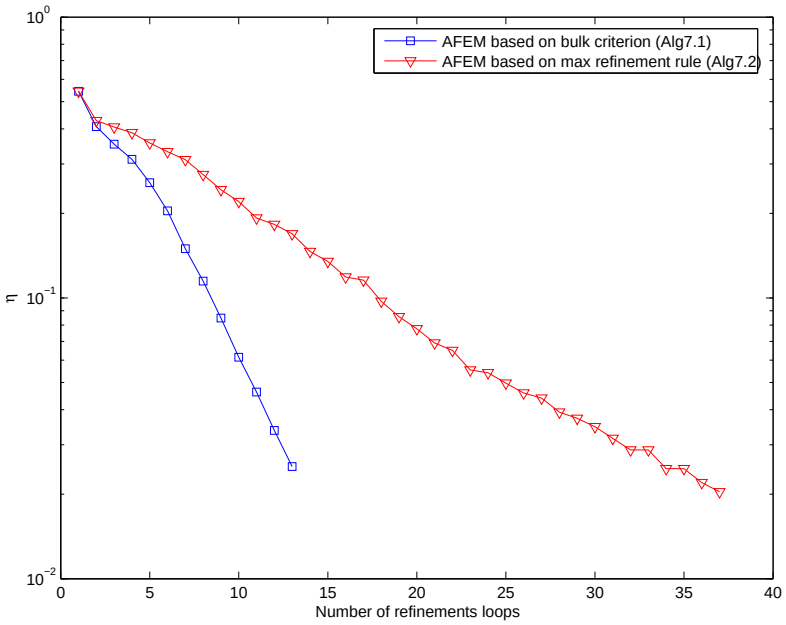

FIGURE 14. Example 7.2: Convergence history of η_ℓ with respect to the number of refinement loops for the adaptive finite element refinements based on the bulk criterion (1.3) computed by Algorithm 7.1 with $\Theta = 0.5$, and on the max refinement rule (1.2) computed by Algorithm 7.2 with $\Theta = 0.5$. The AFEM based on (1.3) performs with a linear convergence rate that is better than the one displayed by the AFEM based on (1.2).

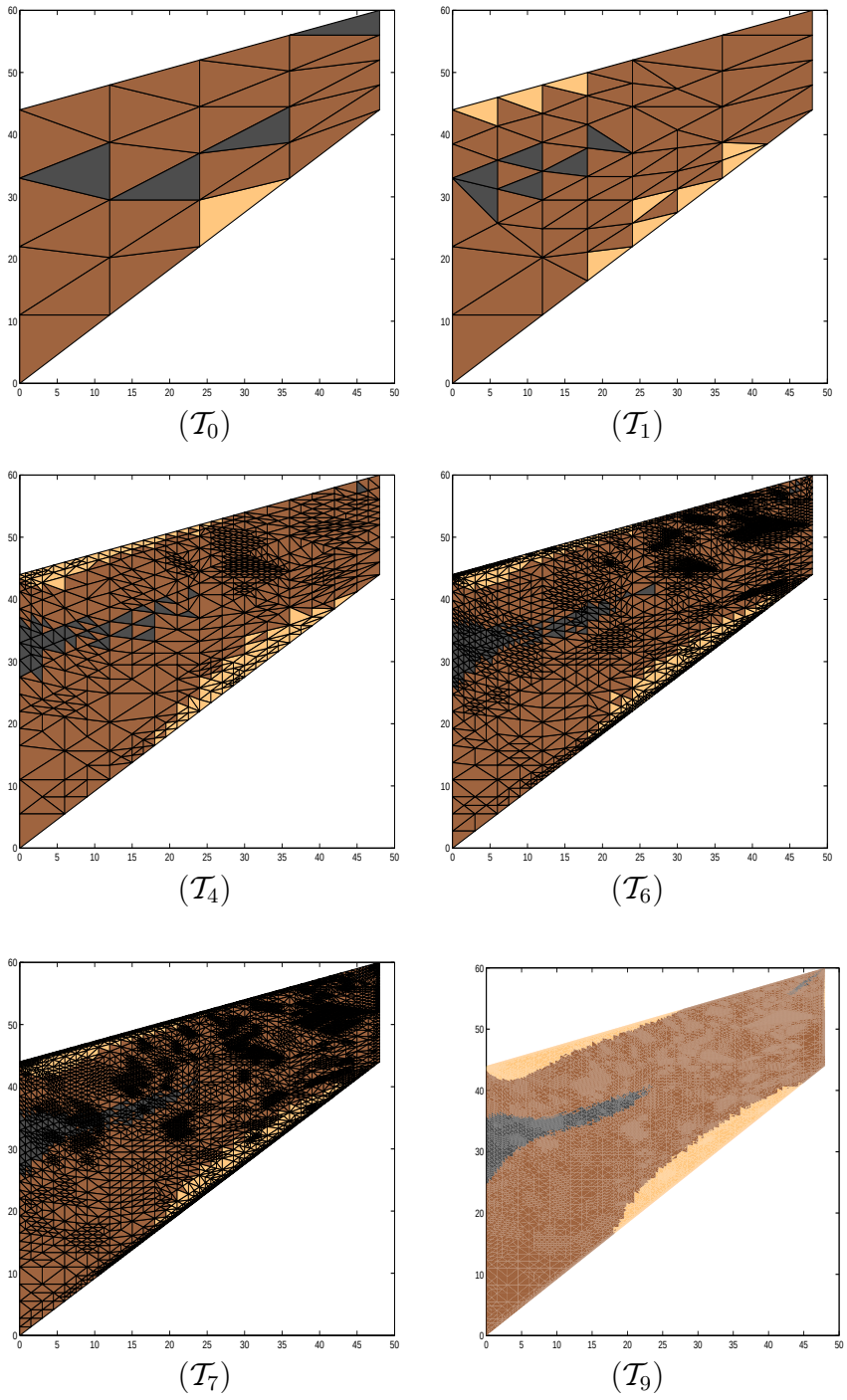

FIGURE 15. Example 7.2: Adapted triangulations $\mathcal{T}_0$, $\mathcal{T}_1$, $\mathcal{T}_4$, $\mathcal{T}_6$, $\mathcal{T}_7$, $\mathcal{T}_9$ for the Cook's membrane generated with the Algorithm 7.1 with $\Theta = 1/2$. Notice a local higher refinement towards the upper left corner where change of boundary condition soccur and at the right end where point loads are applied. For visualization reason, $\mathcal{T}_9$ does not visualize the underlying mesh. Color legend: black=elastic, dark gray=first yield activated, light gray=second yield activated.

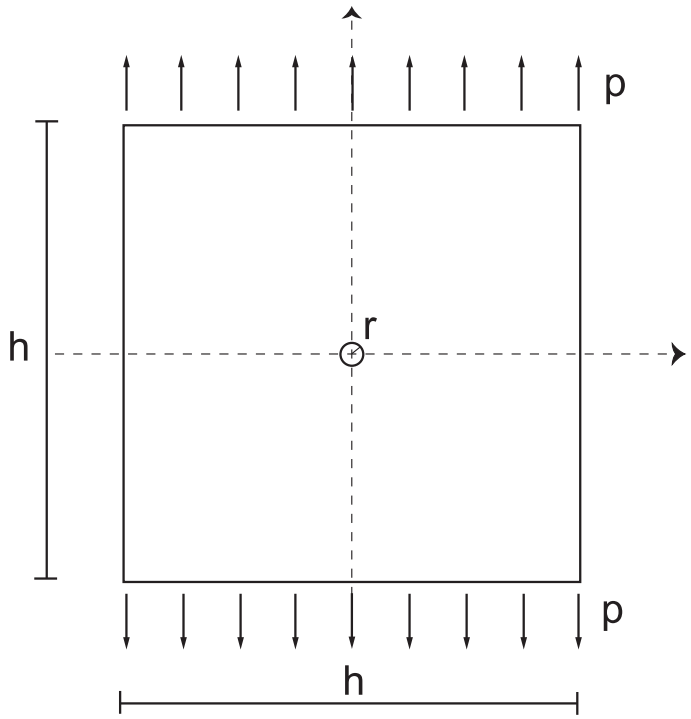

$h = 200$ $r = 10$

$p = 450$ $p_{cr} = 515.5$

$E = 206899.94$ $\nu = 0.29$

$\sigma_y = 450.00$

FIGURE 16. Example 7.3: Geometry for a rectangular domain with a hole under plane strain condition and using perfect plasticity [36].

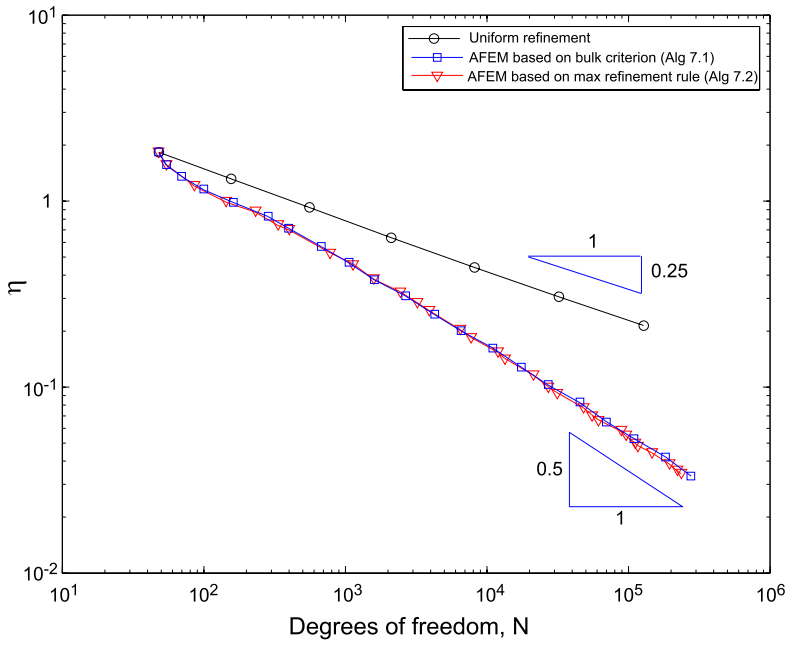

FIGURE 17. Example 7.3: Convergence history of η_ℓ for uniform and adaptive finite element refinements based on the bulk criterion (1.3) computed by Algorithm 7.1 with $\Theta = 0.5$, and on the max refinement rule (1.2) computed by Algorithm 7.2 with $\Theta = 0.5$. Each adaptive algorithm performs with a convergence rate with respect to the number of degree of freedom of about 0.5 in contrast to 0.25 for uniform refinement. This corresponds to the empirical convergence rate of 1 and 0.5, respectively, with respect to a (uniform) mesh size h.

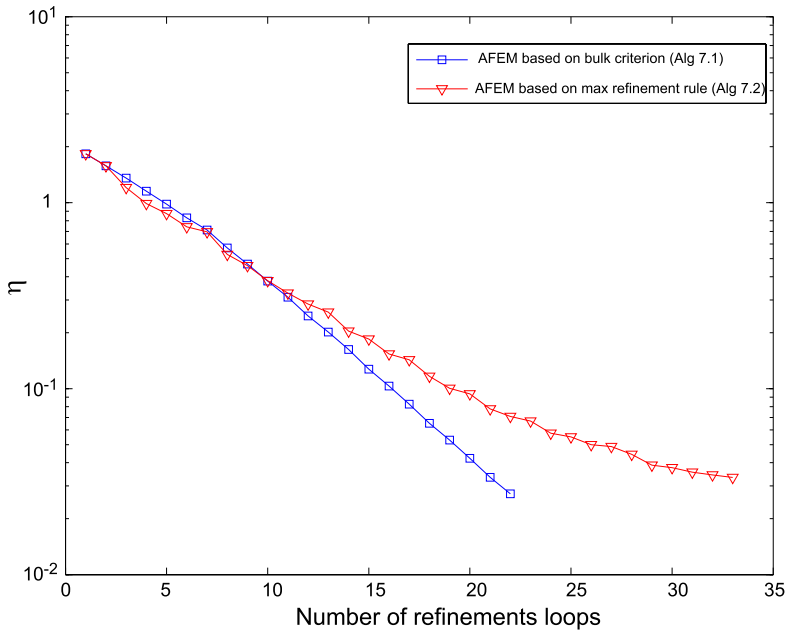

FIGURE 18. Example 7.3: Convergence history of η_ℓ with respect to the number of refinement loops for the adaptive finite element refinements based on the bulk criterion (1.3) computed by Algorithm 7.1 with $\Theta = 0.5$, and on the max refinement rule (1.2) computed by Algorithm 7.2 with $\Theta = 0.5$). The AFEM based on (1.3) performs with a linear convergence rate that is better than the one displayed by the AFEM based on (1.2).